On a Solution of the Closure Problem for Dry Convective Boundary Layer Turbulence and Beyond

VLADIMIR M. GRYANIK[a,b] AND JÖRG HARTMANN[a]

[a] *Alfred-Wegener-Institut Helmholtz-Zentrum für Polar und Meeresforschung, Bremerhaven, Germany*
[b] *A. M. Obukhov Institute of Atmospheric Physics, Russian Academy of Sciences, Moscow, Russia*

ABSTRACT: We consider the closure problem of representing the higher-order moments (HOMs) in terms of lower-order moments, a central feature in turbulence modeling based on the Reynolds-averaged Navier–Stokes (RANS) approach. Our focus is on models suited for the description of asymmetric, nonlocal, and semiorganized turbulence in the dry atmospheric convective boundary layer (CBL). We establish a multivariate probability density function (PDF) describing populations of plumes that are embedded in a sea of weaker randomly spaced eddies, and apply an assumed delta-PDF approximation. The main content of this approach consists of capturing the bulk properties of the PDF. We solve the closure problem analytically for all relevant HOMs involving velocity components and temperature and establish a hierarchy of new non-Gaussian turbulence closure models of different content and complexity ranging from analytical to semianalytical. All HOMs in the hierarchy have a universal and simple functional form. They refine the widely used Millionshchikov closure hypothesis and generalize the famous quadratic skewness–kurtosis relationship to higher order. We examine the performance of the new closures by comparison with measurement, LES, and DNS data and derive empirical constants for semianalytical models, which are best for practical applications. We show that the new models have a good skill in predicting the HOMs for atmospheric CBL. Our closures can be implemented in second-, third-, and fourth-order RANS turbulence closure models of bi-, tri-, and four-variate levels of complexity. Finally, several possible generalizations of our approach are discussed.

KEYWORDS: Atmosphere; Boundary layer; Convective parameterization; Eddies; Parameterization; Turbulence; Updrafts/downdrafts

1. Introduction and background

The Reynolds-averaged Navier–Stokes (RANS) turbulence model (e.g., Monin and Yaglom 2007a,b) is a powerful tool for studying the convective boundary layer (CBL). Any RANS model must solve the turbulence closure problem of representing higher-order moments (HOMs) in terms of lower-order moments. This problem is still unsolved for the atmospheric CBL due to the complexity of the CBL turbulence structure. It is proven that only third- and higher-order closure (HOC) models are able to describe CBL turbulence statistics properly (Mellor and Yamada 1982; Canuto et al. 1994; Mironov and Machulskaya 2017). The reason is the asymmetry of CBL turbulence and its nonlocal and semiorganized structure (e.g., Deardorff 1970; Hunt 1984; Wyngaard 1987). The asymmetry is due to the main forcing at the surface leading to the emergence of coherent features, namely, the evolution of plumes. These plumes are convective circulation cells roughly of the size of the boundary layer height z_i in the vertical and of several z_i in the horizontal direction. The updraft motions form a localized core, which is surrounded by wide downdraft motions. This layer of large-scale mixing is sandwiched by two layers of small-scale mixing. In the surface

layer mixing is dominated by eddies of the sizes $l \sim z$ in the vertical and of several l in the horizontal direction. Here, z is the distance to the underlying surface. Above the mixing layer, in the entrainment zone, mixing is also due to small-scale eddies generated by wind shear and due to breaking of internal gravity waves.

Our main target is the solution of the closure problem for HOC RANS models of convective turbulence. We apply the so-called assumed probability density function (PDF) approach, more precisely, the assumed delta-PDF approximation.

The assumed PDF approach is a straightforward one and can be traced back to the Millionshchikov hypothesis (Millionshchikov 1941), where the PDF is quasi Gaussian such that the fourth-order moments (FOMs) are Gaussian although the third-order moments (TOMs) are nonzero. Thus the FOMs are expressed in terms of second-order moments (SOMs). The widely used Gram–Charlier PDF (Monin and Yaglom 2007a,b) formalizes the Millionshchikov hypothesis as a perturbative theory of small deviations of turbulence statistics from the Gaussian distribution. The obvious advantage of the general assumed PDF approach is that the PDFs depend on a finite set of N parameters, which can be determined using the N lower-order moments, *the irreducible moments*. The moments are irreducible in the sense that all other HOMs based on this PDF are expressed in terms of these N moments. If so, the system of RANS equations becomes closed, and only N dynamic equations for the irreducible moments become relevant for the description of the turbulent flow.
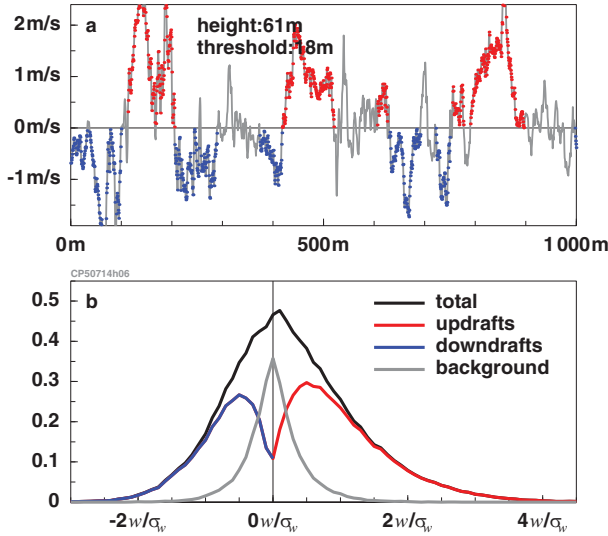
FIG. 1. Illustration of a PDF superposition of up- and downdrafts and background motion. The figure shows actual measurement data of the vertical wind velocity recorded during a 100-km-long aircraft traverse at low level (height of 61 m above ground) through a well-developed convective boundary layer. (a) An excerpt of 1000-m length of the vertical wind velocity fluctuations. Note that the fluctuations are calculated with respect to the mean over the entire flight leg. Portions where the data change sign on a horizontal distance shorter than the threshold (here: 18 m) are marked by gray color. Red and blue marks up- and downdrafts, respectively, as defined by a horizontal persistence of at least the length of the threshold of 18 m. (b) The corresponding frequency distribution of the up- and downdrafts (red and blue), the background (gray), and the total (black). The full distribution (black) is the sum of the three components (blue, red, and gray).

A PDF model suitable to describe convective turbulence must explicitly include a bimodal part for the large-scale plumes (updrafts and downdrafts) and a unimodal part for the small-scale weak eddies. We illustrate this decomposition feature in Fig. 1. The upper graph shows a section of a space series of vertical velocity fluctuations measured at low level in a convective boundary layer. The signal was chosen for no particular reasons other than that it reflects the typical fluctuations of the vertical velocity in convective conditions. The data series is split based on sign persistence on a horizontal scale. Portions where the sign changes on a horizontal distance shorter than a threshold length l are defined as background. Here l is the characteristic horizontal scale of the eddies, such that $\min(z, L) \leq l \ll z_i$, where $L = -\Theta u_*^3 / \kappa g \overline{w' \theta_0'}$ is the Monin–Obukhov length (Obukhov 1946), $u_* = \left(\overline{w' u_0'}^2 + \overline{w' v_0'}^2 \right)^{1/2}$ is the friction velocity, $\overline{w' u_0'}$, $\overline{w' v_0'}$ and $\overline{w' \theta_0'}$ are the surface values of the momentum and heat fluxes, κ is the Karman constant, g is the acceleration due to gravity, and Θ the reference temperature. Here and in the following the Reynolds averages of velocity components u', v', and w' and temperature fluctuations θ' are denoted by overline, but the corresponding model dependent averages are denoted by angle brackets. All longer stretches in Fig. 1a are

either updraft fluctuation w_u for $w' > 0$ or downdraft fluctuation w_d for $w' < 0$. Figure 1b shows the splitting in terms of the univariate PDF $P(w')$. The black curve is the PDF of the full signal. The red curve corresponds to updrafts, the blue one to downdrafts and gray is the background.

The PDF $P(w')$ has the functional form

$$P(w') = p_u G_u(w') + p_d G_d(w') + p_0 G_0(w'), \qquad (1)$$

where p_u, p_d, and p_0 are the probabilities (area coverages) and $G_u(w')$, $G_d(w')$, and $G_0(w')$ are shape functions for updrafts, downdrafts, and background, respectively, cf. Hunt (1984). The function $G_u(w')$ is such that $G_u(w') = 0$ for negative fluctuations $w' < 0$, and the shape function $G_d(w') = 0$ for positive fluctuations $w' > 0$. All shape functions are normalized to unity. Therefore, integrating Eq. (1) over all fluctuations w' leads to the normalization condition

$$p_u + p_d + p_0 = 1. \qquad (2)$$

The basis of the assumed delta-PDF approximation (ADA) is to approximate the full PDF by a small number of delta functions. In this approach any PDF of the functional form (1) can be approximated as

$$P(w') = p_u \delta(w' - w_u) + p_d \delta(w' - w_d) + p_0 \delta(w') \qquad (3)$$

with the normalization condition (2), where $\delta(\phi)$ is the Dirac delta function, and w_u and w_d are the mean updraft and downdraft velocities.

The main content of ADA consists in capturing of the bulk properties of the PDF, see Fig. 1b. Figuratively speaking, the ADA based PDF is a skeleton of any PDF. Approximating a continuous PDF by delta functions allows developing an analytically tractable description. This approximation is complementary to one focusing on the properties of a particular shape of a PDF (e.g., Millionshchikov 1941; Larson and Golaz 2005; Firl and Randall 2015; and references therein).

Figure 2 shows an illustration of using the ADA concept for the solution of the closure problem.

It is obvious, that with only three probability parameters p_u, p_d, and p_0 and two velocities w_u and w_d the PDF (3) is not yet able to describe the difference of velocity and temperature fluctuations. Therefore, Gryanik and Hartmann (2002, hereafter GH02) introduced a 2-scale mass flux model based on the bivariate PDF $P(w', \theta')$ and Gryanik et al. (2005, hereafter GH05), extended it to a 4-scale model using the PDF $P(w', \theta', u', v')$. GH05 only derived closures for TOMs and FOMs and solved the closure problem approximately, using a so-called universality hypothesis. This claims that the actual FOMs are the result of linear interpolation between the two limits of very skewed (mass-flux) and nonskewed (Gaussian) turbulence. Thus, the universality hypothesis states that

$$\overline{w'^4} = 3 \left(1 + \frac{1}{3} S_w^2 \right) \overline{w'^2}^2, \qquad (4a)$$

$$\overline{w'^3 \theta'} = 3 \left(1 + \frac{1}{3} S_w^2 \right) \overline{w'^2} \; \overline{w' \theta'}, \qquad (4b)$$
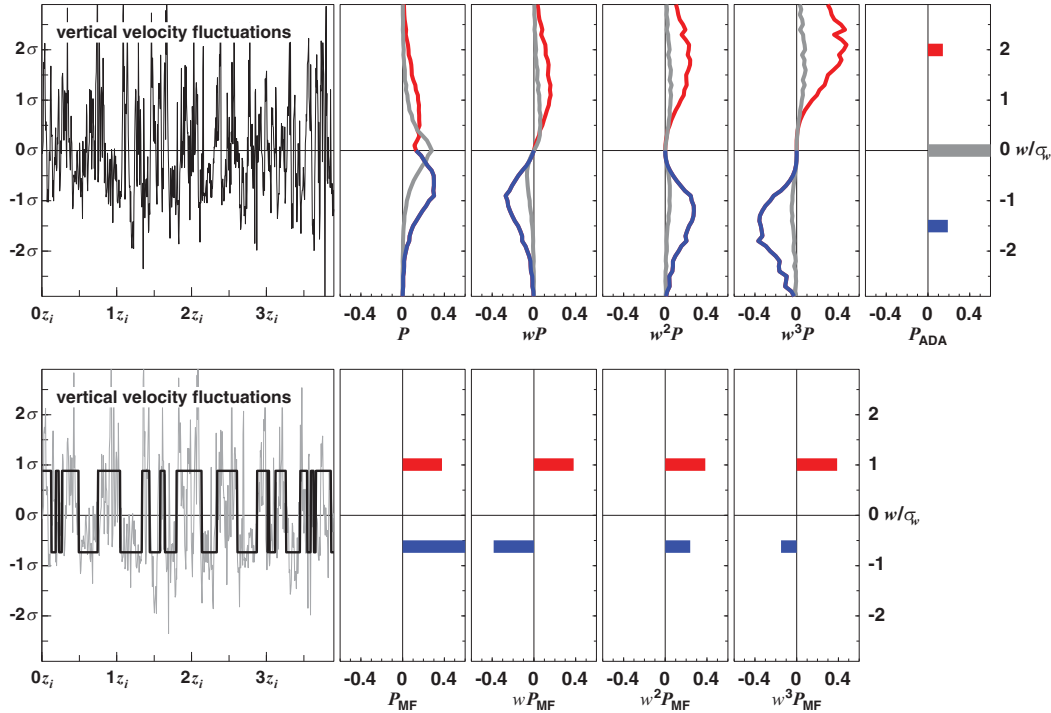
FIG. 2. An illustration of the ADA concept. (top) An arbitrary excerpt of a recording of the vertical velocity at low level in a convective boundary layer. The ordinate is scaled with the standard deviation σ_w and the abscissa with the length scale z_i. The corresponding normalized probability density distributions P of this data is shown over the same ordinate to the right in red for $w > 0$ and in blue for $w < 0$; gray marks the background (cf. Fig. 1). To illustrate their respective contributions to the irreducible moments, P is also shown multiplied with increasing powers of w. Note that the background contribution loses influence with increasing power and the peaks move to larger values. To the very right the delta-PDFs are shown symbolically, since actual δ functions have infinite amplitude and zero width. (bottom) For comparison with the traditional mass-flux concept, the same turbulence data in light gray and their mass-flux representation (thick black). To the right the mass-flux probabilities are shown multiplied with increasing powers of w in analogy to the above graphs.

$$\overline{w'^2\theta'^2} = \left(1 + 2C_{w\theta}^2 + C_{w\theta}S_wS_\theta\right)\overline{w'^2}\ \overline{\theta'^2}, \tag{4c}$$

$$\overline{w'\theta'^3} = 3\left(1 + \frac{1}{3}S_\theta^2\right)\overline{\theta'^2}\ \overline{w'\theta'}, \tag{4d}$$

$$\overline{\theta'^4} = 3\left(1 + \frac{1}{3}S_\theta^2\right)\overline{\theta'^2}^2, \tag{4e}$$

where $C_{w\theta} = \overline{w'\theta'}/\overline{w'^2}^{1/2}\overline{\theta'^2}^{1/2}$ is a correlation coefficient, $S_w = \overline{w'^3}/\overline{w'^2}^{3/2}$ and $S_\theta = \overline{\theta'^3}/\overline{\theta'^2}^{3/2}$ are the skewnesses. The universality hypothesis refines the Millionshchikov hypothesis, which is often used in RANS turbulence models. GH02 and GH05 also introduced an extended universality hypothesis that allows for a variation of the constants, but keeps the functional form predicted by the universality hypothesis.

Both the universality and the extended universality hypothesis have shown good skills in describing the results of field measurements (Hartmann et al. 1999; Lenschow et al. 2012; McNicholas and Turner 2014), of numerical simulations of the CBL (Raasch and Schröter 2001; Cheng et al. 2005; Larson and Golaz 2005; Ilyushin 2018) and, moreover, of deep convection in the ocean (Losch 2004) and in the sun and stars (Kupka and Robinson

2007; Kupka and Muthsam 2017; Cai 2018) and even of engineering flows (Waggy et al. 2016; Hsieh and Biringen 2018). Currently, the closure equation, Eq. (4e), is used in the research version of the NWP model Consortium for Small-Scale Modeling (COSMO; Mironov and Machulskaya 2017). These are unexpected and amazing results, keeping in mind how wide the spectrum of these turbulent flow regimes is and how many assumptions were made in the derivation of the closure equations.

The results described above motivate us to ask the following questions: Where are the roots of the universal features of this closure? Can the number of assumptions be reduced while the closure still captures all important ingredients of the earlier ones, i.e., how simple is simple enough? Can the results be generalized to multivariate HOMs? These questions specify the goals of our research as follows.

The first goal is to establish the ADA-based multivariate PDF that describes a population of plumes embedded in a sea of weaker randomly spaced eddies of small scales forming a turbulent background.

The second goal is to solve analytically the closure problem for all relevant multivariate HOMs using the new PDF as basis. This solution will clarify several issues, such as the

functional form of HOMs in advanced RANS closure models, an impact of interplay of coherent structures with a background on closures for HOMs and a generalization of the famous skewness–kurtosis relationships to higher orders.

The third goal of our research is to establish a hierarchy of new HOM closure models of different content and complexity, ranging from analytical to semianalytical models. The hierarchy appears naturally because the solution of our closure problem, as well as any other, is not unique. In particular, we will show how these models unify and/or refine some of the closure models suggested earlier.

The fourth goal is to examine the performance of the new closures by comparison with data from measurements, LES, and DNS. We present results of testing many multivariate HOMs not considered before and derive empirical constants for semianalytical models, which are most well suited for practical use in RANS models.

Finally, comparison of the results from our closure models with models focusing on a specific shape of PDFs will explicitly show what was actually done beyond the basic bulk features in the models, and which fundamentally important bulk features were neglected in the models. The comparison can provide the key for understanding possible directions for developing more advanced RANS closure models.

This paper is organized as follows. Sections 2 to 8 present the theory, including the analytical exact solution for all multivariate HOMs. Sections 9 to 11 present the results of a comparison of the theory with datasets from measurements, LES, and DNS. In sections 12 and 13 a new semianalytical closure model for practical use is established. Section 14 includes a summary of our main results, a discussion of possible generalizations and applications.

2. Multivariate 17-delta-PDF and moments

We apply the ADA method to the PDF of four variables w', θ', u', and v', and approximate the multivariate PDF $P(w', \theta', u', v')$ by a delta-PDF. The 17-delta-PDF follows as a superposition of the 16 deltas in each respective hexadecant of our four-dimensional system multiplied by their individual probability and additionally the probability of the background.

Thus, our proposal reads

$$
\begin{aligned}
P(w', \theta', u', v') =\ & p_{uhfr}\delta(w' - w_u)\delta(\theta' - \theta_h)\delta(u' - u_f)\delta(v' - v_r) \\
& + p_{dcfr}\delta(w' - w_d)\delta(\theta' - \theta_c)\delta(u' - u_f)\delta(v' - v_r) \\
& + p_{ucfr}\delta(w' - w_u)\delta(\theta' - \theta_c)\delta(u' - u_f)\delta(v' - v_r) \\
& + p_{dhfr}\delta(w' - w_d)\delta(\theta' - \theta_h)\delta(u' - u_f)\delta(v' - v_r) \\
& + p_{uhbr}\delta(w' - w_u)\delta(\theta' - \theta_h)\delta(u' - u_b)\delta(v' - v_r) \\
& + p_{dcbr}\delta(w' - w_d)\delta(\theta' - \theta_c)\delta(u' - u_b)\delta(v' - v_r) \\
& + p_{ucbr}\delta(w' - w_u)\delta(\theta' - \theta_c)\delta(u' - u_b)\delta(v' - v_r) \\
& + p_{dhbr}\delta(w' - w_d)\delta(\theta' - \theta_h)\delta(u' - u_b)\delta(v' - v_r) \\
& + p_{uhfl}\delta(w' - w_u)\delta(\theta' - \theta_h)\delta(u' - u_f)\delta(v' - v_l) \\
& + p_{dcfl}\delta(w' - w_d)\delta(\theta' - \theta_c)\delta(u' - u_f)\delta(v' - v_l) \\
& + p_{ucfl}\delta(w' - w_u)\delta(\theta' - \theta_c)\delta(u' - u_f)\delta(v' - v_l) \\
& + p_{dhfl}\delta(w' - w_d)\delta(\theta' - \theta_h)\delta(u' - u_f)\delta(v' - v_l) \\
& + p_{uhbl}\delta(w' - w_u)\delta(\theta' - \theta_h)\delta(u' - u_b)\delta(v' - v_l) \\
& + p_{dcbl}\delta(w' - w_d)\delta(\theta' - \theta_c)\delta(u' - u_b)\delta(v' - v_l) \\
& + p_{ucbl}\delta(w' - w_u)\delta(\theta' - \theta_c)\delta(u' - u_b)\delta(v' - v_l) \\
& + p_{dhbl}\delta(w' - w_d)\delta(\theta' - \theta_h)\delta(u' - u_b)\delta(v' - v_l) \\
& + p_0\delta(w')\delta(\theta')(\theta')\delta(u')(u')\delta(v').
\end{aligned}
$$

(5)

The PDF is normalized as

$$ p_S + p_0 = 1, \tag{6a} $$

$$
\begin{aligned}
p_S =\ & p_{uhfr} + p_{dcfr} + p_{ucfr} + p_{dhfr} + p_{uhbr} + p_{dcbr} + p_{ucbr} \\
& + p_{dhbr} + p_{uhfl} + p_{dcfl} + p_{ucfl} + p_{dhfl} + p_{uhbl} + p_{dcbl} \\
& + p_{ucbl} + p_{dhbl},
\end{aligned}
$$

(6b)

where p_S describes the concentration of coherent structures, and p_0 the background. The PDF (5) introduces a detailed description of coherent structures, because it specifies 8 independent modes describing coherent structures and correspondingly 16 area coverage parameters. The deviation from the mean vertical velocity w' is represented by updraft fluctuations w_u and downdraft ones w_d, the deviation from mean temperature θ' by hot and cold fluctuations θ_h and θ_c, the deviation from the mean along-stream velocity u' is described by forward and backward fluctuations u_f and u_b of velocities, and finally the deviation from the mean cross-stream velocity v' by left v_l and right v_r components. Then, for example, the joint probability of hot updraft w_u, θ_h together with the along wind forward component u_f, which deviate to the right v_r in the region $(w' > 0) \wedge (\theta' > 0) \wedge (u' > 0) \wedge (v' > 0)$, is denoted p_{uhfr}. For more details, see GH05. Thus, using PDF (5) the complex morphology of convective turbulent flows is described by 25 parameters.

The PDF (5) is the simplest, but nontrivial, delta-PDF of four variables. Being formed by a linear superposition of the delta-PDFs for w', θ', u', and v', the PDF (5) potentially can approximate

- isotropic turbulence at small scales, where all velocity components are of the same order $w_u \sim -w_d \sim -u_f \sim -u_b \sim -v_r \sim -v_l$, temperature fluctuations are similar $\theta_h \sim -\theta_c$, and all individual probabilities have approximately equal values;
- highly anisotropic large-scale turbulence represented by populations of plumes in the mixed layer, dominated by vertical velocity fluctuations $w_u \gg -w_d \gg u_f$, u_b, v_r, v_l, strong hot updraft motions $\theta_h \gg -\theta_c$, and high correlation between vertical velocity and temperature;
- highly anisotropic turbulence dominated by horizontal velocity fluctuations u_f, $-u_b$, v_r, $-v_l \gg w_u$, $-w_d$ with a dominance of cold downdrafts $\theta_h \ll -\theta_c$ and very low probabilities involving vertical velocities in the surface layer and in the inversion;
- and even very weak turbulence regimes in the stably stratified fluid aloft where both velocity and temperature fluctuations are very small.

Thus, the PDF is desirable to account for full range of physically relevant parameters.

Using PDF (5) in the definition of the moments $\langle M_{nmlk} \rangle = \langle w'^n \theta'^m u'^l v'^k \rangle$, where n, m, k, and l are integers ≥ 0, one can easily obtain these slightly cumbersome but explicit formula for the moments:

TABLE 1. Hierarchy of delta-PDF models. The first column shows the level of complexity of the model. The second column presents the abbreviation of the model for the given level of complexity. The third column describes the number of corresponding models, and the fourth column shows the number of parameters, which should be determined to specify the PDF. The first term refers to the number of probabilities and the second to the number of positions. The last column refers to the equations representing the closure of the model. The values of the parameter p_S in the equation are the same for all levels.

Level	Model	No. of models	No. of variables	Closure equations
4	Quadrivariate	1	$17 + 8 = 25$	(44), (33), (27)
3	Trivariate	4	$9 + 6 = 15$	(40), (33), (27)
2	Bivariate	6	$5 + 4 = 9$	(32), (33), (27)
1	Univariate	4	$3 + 2 = 5$	Part of levels 2–4

$$
\begin{aligned}
\langle M_{nmlk} \rangle = &+ p_{uhfr} w_u^n \theta_h^m u_f^l v_r^k + p_{dcfr} w_d^n \theta_c^m u_f^l v_r^k + p_{ucfr} w_u^n \theta_c^m u_f^l v_r^k + p_{dhfr} w_d^n \theta_h^m u_f^l v_r^k + p_{uhbr} w_u^n \theta_h^m u_b^l v_r^k + p_{dcbr} w_d^n \theta_c^m u_b^l v_r^k \\
&+ p_{ucbr} w_u^n \theta_c^m u_b^l v_r^k + p_{dhbr} w_d^n \theta_h^m u_b^l v_r^k + p_{uhfl} w_u^n \theta_h^m u_f^l v_l^k + p_{dcfl} w_d^n \theta_c^m u_f^l v_l^k + p_{ucfl} w_u^n \theta_c^m u_f^l v_l^k + p_{dhfl} w_d^n \theta_h^m u_f^l v_l^k \\
&+ p_{uhbl} w_u^n \theta_h^m u_b^l v_l^k + p_{dcbl} w_d^n \theta_c^m u_b^l v_l^k + p_{ucbl} w_u^n \theta_c^m u_b^l v_l^k + p_{dhbl} w_d^n \theta_h^m u_b^l v_l^k + p_0 \delta_{n0} \delta_{m0} \delta_{l0} \delta_{k0},
\end{aligned} \tag{7}
$$

with the Kronecker symbol $\delta_{ij} = 1$ if $I = j$, and $\delta_{ij} = 0$ if $i \neq j$. The first term is the partial contribution of the updraft, hot, forward, and right fluctuations, the second term is the contribution of the downdraft, cold, forward, and right fluctuations, and so on.

For the zeroth-order moments ($n = m = k = l = 0$) Eq. (7) gives the normalization condition (6a) with (6b). For the first-order ($n = 1$, but $m = k = l = 0$, and similar for m, k, and l indices) Eq. (7) gives the mean value of the fluctuations $\langle w' \rangle$, $\langle \theta' \rangle$, $\langle u' \rangle$, and $\langle v' \rangle$ as

$$
\begin{aligned}
p_u w_u + p_d w_d &= 0, \\
p_h \theta_h + p_c \theta_c &= 0, \\
p_f u_f + p_b u_b &= 0, \\
p_r v_r + p_l v_l &= 0.
\end{aligned} \tag{8}
$$

Finally, note that the PDF $P(w', \theta', u', v')$ [Eq. (5)] describes the fluctuations, i.e., the deviations from the mean flow fields $\langle w \rangle$, $\langle \theta \rangle$, $\langle u \rangle$, and $\langle v \rangle$. The PDF $P(w, \theta, u, v)$ of flow fields w, θ, u, v is obtained by shift of variables, i.e., $P(w, \theta, u, v) = P(\langle w \rangle + w', \langle \theta \rangle + \theta', \langle u \rangle + u', \langle v \rangle + v')$.

3. A guide for the solution

The solution of the closure problem for the 17-delta-PDF (5) consists of solving the system of algebraic nonlinear Eqs. (7) for the 25 parameters of the PDF (8 positions of delta functions and $16 + 1$ probabilities) using selected moments of low order ("the irreducible moments") and then expressing the other HOMs in terms of these irreducible moments. If the equations for the normalization condition (6a) with (6b) and the equation for the mean values of the fluctuations (8) are used, the amount of required independent irreducible moments of the order larger than one is equal to 20.

We apply a bottom-up method of solution by establishing a hierarchy of PDFs of different levels of complexity, as given in Table 1, and by deriving the relationships for the parameters of these PDF of different levels.

The most general PDF (5) represents level 4 of the hierarchy and is described in the previous section.

Formally, on level 3 there are four trivariate 9-delta-PDFs: $P(w', u', v')$, $P(w', u', v')$, $P(w', \theta', v')$, and $P(\theta', u', v')$. They are obtained by integration of (5) over the variables v', θ', u', or w', respectively. For example, the trivariate PDF $P(w', \theta', v')$ is obtained by integrating (5) over the along-wind component u'. The functional form of the trivariate PDF is similar to (5), but with only three variables involved and only 9 probabilities and 6 positions remaining. Thus the probability p_{uhr} of hot updrafts turned to the right are given as

$$
p_{uhr} = p_{uhfr} + p_{uhbr}. \tag{9}
$$

Similar formulas hold for the other seven trivariate probabilities. Each of the remaining probabilities is the sum of two, becoming hidden after integration. The sum of all probabilities gives the normalization condition

$$
\begin{aligned}
& p_{uhr} + p_{uhl} + p_{ucr} + p_{ucl} + p_{dhr} + p_{dhl} + p_{dcr} + p_{dcl} + p_0 \\
& = 1,
\end{aligned} \tag{10}
$$

where the individual probabilities are expressed as sums of quadrivariate probabilities, similar to Eq. (9).

There are six bivariate 5-delta-PDFs (representing level 2 in Table 1) where each is obtained by integration over two variables. E.g., averaging over the horizontal velocity components the bivariate PDF

$$
\begin{aligned}
P(w', \theta') = &+ p_{uh} \delta(w' - w_u) \delta(\theta' - \theta_h) \\
&+ p_{uc} \delta(w' - w_u) \delta(\theta' - \theta_c) \\
&+ p_{dh} \delta(w' - w_d) \delta(\theta' - \theta_h) \\
&+ p_{dc} \delta(w' - w_d) \delta(\theta' - \theta_c) \\
&+ p_0 \delta(w') \delta(\theta')
\end{aligned} \tag{11}
$$

with the normalization condition

$$p_{uh} + p_{dc} + p_{uc} + p_{dh} + p_0 = 1 \qquad (12)$$

follows. Such a PDF provides a minimal model for the free convection regime, which is characterized by the presence of populations of plumes organized in quasi-regular cells. In this case one can assume homogeneity and isotropy of the convective turbulence in both horizontal directions. There are four bimodal probabilities, which can be expressed in terms of trivariate probabilities as

$$p_{uh} = p_{uhf} + p_{uhb} = p_{uhr} + p_{uhl} \qquad (13)$$

and similar formulas for the probabilities p_{dc}, p_{uc}, and p_{dh}. In analogy, the other five bivariate PDFs (see Table 1) can easily be obtained by renaming of the indices in Eq. (11).

At the lowest level of hierarchy (see Table 1) we have four univariate 3-delta-PDFs: $P(w')$, $P(\theta')$, $P(u')$, and $P(v')$. These PDFs, as the simplest ones, were often used in the past, e.g., by Wyngaard (1987) for vertical velocity fluctuations. Only three probabilities and two positions describe this delta-PDF. They are related to probabilities of higher levels. Thus, the probability of updrafts consists of the sum of 2 probabilities

$$p_u = p_{uh} + p_{uc} = p_{uf} + p_{ub} = p_{ur} + p_{ul} \qquad (14)$$

for bivariate PDFs, of the sum of 4 probabilities

$$\begin{aligned} p_u &= p_{uhf} + p_{uhb} + p_{ucf} + p_{ucb} \\ &= p_{uhf} + p_{ucb} + p_{uhb} + p_{ucb} \\ &= p_{uhr} + p_{ucr} + p_{uhl} + p_{ucl} \end{aligned} \qquad (15)$$

for trivariate PDFs, and finally of the sum of 8 probabilities

$$\begin{aligned} p_u &= + p_{uhfr} + p_{ucfr} + p_{uhbr} + p_{ucbr} \\ &\quad + p_{uhfl} + p_{ucfl} + p_{uhbl} + p_{ucbl} \end{aligned} \qquad (16)$$

for the most general PDF (5). Each of the other probabilities p_h, p_f, and p_r is derived similarly.

The procedure of the solution consists of these steps:

1) Establish the factorized functional form of the HOMs in terms of the width of the PDF (in section 4).
2) Solve for the bivariate moments using one of the bivariate 5-delta-PDFs. Extrapolate the results to all bivariate PDFs (section 5).
3) Solve for the trivariate moments using one of the trivariate 9-delta-PDFs and the results from step 2. Extrapolate the results to all trivariate 5-delta-PDFs (section 6).
4) Solve for the quadrivariate moments using the general quadrivariate 17-delta-PDF and the results from steps 2 and 3 (section 7).
5) Specify the probability p_S (section 8).
6) Identify a connection of the modeled irreducible moments with their corresponding Reynolds moments (section 8).

Step 1 consists of solving for all position in terms of width using the zeroth- and first-order univariate moments.

Steps 2 to 4 include the following:

(i)   Choice of the irreducible moments.
(ii) Solution of the equations for the width and the individual probabilities (except for p_S) in terms of the irreducible moments of the second and third order.
(iii) Solution of the other HOMs in terms of the irreducible moments and p_S, using the results from (i) and (ii).
(iv) Extension of the solution to all members of the same level of hierarchy using the results from (i), (ii), and (iii).

Step 5 completes the formal mathematical solution of the closure problem. Step 6 completes the solution at the physical level, since it relates the model results to measurements, LES and DNS results. The solution of our closure problem is not unique, as the choice of irreducible moments [see steps 2(ii), 3(ii), and 4(ii) of the guide of solution] is not unique. Also, several hypothesis can be used for specification of the parameter p_S, thus step 5 is not unique either. Finally, we stress that our method of solution is new, because we do not use an assumption (often implicit) that *all* the lowest-order moments of a given level of hierarchy must be used before switching to higher levels. The new method does not lead to additional difficulties, because all moments of a given PDF are related to each other.

4. Formulation of HOMs in a factorized form and symmetries

The important characteristic of a PDF is its width. In our case the width is the distance Δ between the δ functions in the direction of the respective variable. There are four such widths for the quadrivariate PDF (5). They are

$$\begin{aligned} \Delta_w &= w_u - w_d, \\ \Delta_\theta &= \theta_h - \theta_c, \\ \Delta_u &= u_f - u_b, \\ \Delta_v &= v_r - v_l. \end{aligned} \qquad (17)$$

All widths are positive.

Combining Eqs. (17) and (8) the positions of delta functions can be related to the widths as

$$\begin{aligned} w_u &= (1 - \hat{p}_u)\Delta_w, & w_d &= -\hat{p}_u\Delta_w, \\ \theta_h &= (1 - \hat{p}_h)\Delta_\theta, & \theta_c &= -\hat{p}_h\Delta_\theta, \\ u_f &= (1 - \hat{p}_f)\Delta_u, & u_b &= -\hat{p}_f\Delta_u, \\ v_r &= (1 - \hat{p}_r)\Delta_v, & v_l &= -\hat{p}_f\Delta_v, \end{aligned} \qquad (18)$$

where

$$\hat{p}_u = p_u/p_S, \quad \hat{p}_d = p_d/p_S \qquad (19)$$

are the conditional probabilities for the vertical velocity components, and similar expressions hold for the probabilities of temperature and horizontal velocity components.

Substituting Eqs. (18) in Eq. (7) and rearranging, the terms for the quadrivariate HOMs follow as

$$
\begin{aligned}
\langle w'^n \theta'^m u'^l v'^k \rangle = p_S \big[& \hat{p}_{uhfr}(1 - \hat{p}_u)^n (1 - \hat{p}_h)^m (1 - \hat{p}_f)^l (1 - \hat{p}_r)^k \\
& + \hat{p}_{uhfl}(1 - \hat{p}_u)^n (1 - \hat{p}_h)^m (1 - \hat{p}_f)^l (-\hat{p}_r)^k \\
& + \hat{p}_{uhbr}(1 - \hat{p}_u)^n (1 - \hat{p}_h)^m (-\hat{p}_f)^l (1 - \hat{p}_r)^k \\
& + \hat{p}_{uhbl}(1 - \hat{p}_u)^n (1 - \hat{p}_h)^m (-\hat{p}_f)^l (-\hat{p}_r)^k \\
& + \hat{p}_{ucfr}(1 - \hat{p}_u)^n (-\hat{p}_h)^m (1 - \hat{p}_f)^l (1 - \hat{p}_r)^k \\
& + \hat{p}_{ucfl}(1 - \hat{p}_u)^n (-\hat{p}_h)^m (1 - \hat{p}_f)^l (-\hat{p}_r)^k \\
& + \hat{p}_{ucbr}(1 - \hat{p}_u)^n (-\hat{p}_h)^m (-\hat{p}_f)^l (1 - \hat{p}_r)^k \\
& + \hat{p}_{ucbl}(1 - \hat{p}_u)^n (-\hat{p}_h)^m (-\hat{p}_f)^l (-\hat{p}_r)^k \\
& + \hat{p}_{dhfr}(-\hat{p}_u)^n (1 - \hat{p}_h)^m (1 - \hat{p}_f)^l (1 - \hat{p}_r)^k \\
& + \hat{p}_{dhfl}(-\hat{p}_u)^n (1 - \hat{p}_h)^m (1 - \hat{p}_f)^l (-\hat{p}_r)^k \\
& + \hat{p}_{dhbr}(-\hat{p}_u)^n (1 - \hat{p}_h)^m (-\hat{p}_f)^l (1 - \hat{p}_r)^k \\
& + \hat{p}_{dhbl}(-\hat{p}_u)^n (1 - \hat{p}_h)^m (-\hat{p}_f)^l (-\hat{p}_r)^k \\
& + \hat{p}_{dcfr}(-\hat{p}_u)^n (-\hat{p}_h)^m (1 - \hat{p}_f)^l (1 - \hat{p}_r)^k \\
& + \hat{p}_{dcfl}(-\hat{p}_u)^n (-\hat{p}_h)^m (1 - \hat{p}_f)^l (-\hat{p}_r)^k \\
& + \hat{p}_{dcbr}(-\hat{p}_u)^n (-\hat{p}_h)^m (-\hat{p}_f)^l (1 - \hat{p}_r)^k \\
& + \hat{p}_{dcbl}(-\hat{p}_u)^n (-\hat{p}_h)^m (-\hat{p}_f)^l (-\hat{p}_r)^k \big] \\
& \times \Delta_w^n \Delta_\theta^m \Delta_u^l \Delta_v^k .
\end{aligned}
\tag{20}
$$

Expression (20) is called a factorized form of the HOMs because it represents the moments as a product of a nondimensional factor (depending on probabilities only) and of products of individual widths in the corresponding powers.

The factorization of moments clarifies the relabeling symmetry of the delta-PDF model (5). This symmetry states that permutations of indices $u \leftrightarrow d$, $h \leftrightarrow c$, $f \leftrightarrow b$, and $r \leftrightarrow l$ lead to the same moments except for the sign factor.

5. Bivariate closures for HOMs

Counting the number of independent parameters of the bivariate PDF (11) we find that bivariate closures can be completed at the level of TOMs. Following the guide for solution the five moments

$$
\langle w'^2 \rangle, \ \langle \theta'^2 \rangle, \ \langle w'\theta' \rangle, \ \langle w'^3 \rangle, \ \langle \theta'^3 \rangle
\tag{21}
$$

can be chosen as independent irreducible moments. All the other can be expressed in terms of these irreducible moments and the probability p_S as a parameter, which will be specified later in section 8.

a. Calculation of bivariate irreducible moments in terms of PDF parameters

The bivariate moments in the vertical velocity and temperature are given by the general Eq. (20) as

$$
\begin{aligned}
\langle w'^n \theta'^m \rangle = p_S \big[& \hat{p}_{uh}(1 - \hat{p}_u)^n (1 - \hat{p}_h)^m + \hat{p}_{uc}(1 - \hat{p}_u)^n (-\hat{p}_h)^m \\
& + \hat{p}_{dh}(-\hat{p}_u)^n (1 - \hat{p}_h)^m + \hat{p}_{dc}(-\hat{p}_u)^n \\
& \times (-\hat{p}_h)^m \big] \Delta_w^n \Delta_\theta^m ,
\end{aligned}
\tag{22}
$$

where the first, second, third, and fourth terms are the partial contributions $\langle w'^n \theta'^m \rangle_{uh}$, $\langle w'^n \theta'^m \rangle_{uc}$, $\langle w'^n \theta'^m \rangle_{dh}$, and $\langle w'^n \theta'^m \rangle_{dc}$, respectively.

Correspondingly the irreducible moments are the second-order moments

$$
\langle w'^2 \rangle = p_S \hat{p}_u (1 - \hat{p}_u) \Delta_w^2 ,
\tag{23a}
$$

$$
\langle \theta'^2 \rangle = p_S \hat{p}_h (1 - \hat{p}_h) \Delta_\theta^2 ,
\tag{23b}
$$

$$
\langle w'\theta' \rangle = p_S (\hat{p}_{uh} - \hat{p}_u \hat{p}_h) \Delta_w \Delta_\theta ,
\tag{23c}
$$

and third-order moments

$$
\langle w'^3 \rangle = p_S \hat{p}_u (1 - \hat{p}_u)(1 - 2\hat{p}_u) \Delta_w^3 ,
\tag{23d}
$$

$$
\langle \theta'^3 \rangle = p_S \hat{p}_h (1 - \hat{p}_h)(1 - 2\hat{p}_h) \Delta_\theta^3 ,
\tag{23e}
$$

The physical meaning of these moments is clear from the lowest-order normalized moments, the correlation coefficient

$$
\langle C \rangle_{w\theta} = \frac{\langle w'\theta' \rangle}{\langle w'^2 \rangle^{1/2} \langle \theta'^2 \rangle^{1/2}} = \frac{\hat{p}_{uh} - \hat{p}_u \hat{p}_h}{\sqrt{\hat{p}_u (1 - \hat{p}_u) \hat{p}_h (1 - \hat{p}_h)}},
\tag{24}
$$

and the normalized third-order moments—the skewnesses of vertical velocity and temperature:

$$
\langle S \rangle_w = \frac{\langle w'^3 \rangle}{\langle w'^2 \rangle^{3/2}} = \frac{1}{\sqrt{p_S}} \frac{1 - 2\hat{p}_u}{\sqrt{\hat{p}_u (1 - \hat{p}_u)}},
\tag{25a}
$$

$$
\langle S \rangle_\theta = \frac{\langle \theta'^3 \rangle}{\langle \theta'^2 \rangle^{3/2}} = \frac{1}{\sqrt{p_S}} \frac{1 - 2\hat{p}_h}{\sqrt{\hat{p}_h (1 - \hat{p}_h)}}.
\tag{25b}
$$

The correlation coefficient (24), correspondingly the heat flux, (23c), can be positive or negative depending on the sign of $\hat{p}_{uh} - \hat{p}_u \hat{p}_h$. This allows resolving the problems of negative fluxes in the entrainment zone, appearing in conventional mass flux models. Similarly, Eqs. (25a) and (25b) allow resolving the problems of the difference of vertical velocity and temperature skewnesses without additional assumptions, because $\hat{p}_h \neq \hat{p}_u$. One can also see from these equations that an unskewed flow corresponds to $\hat{p}_u = \hat{p}_h = 1/2$. The skewness is positive for $\hat{p}_u < 1/2$ and $\hat{p}_h < 1/2$, and negative for $\hat{p}_u > 1/2$ and $\hat{p}_h > 1/2$.

b. Calculation of the PDF parameters in terms of the irreducible moments and p_S

To find the PDF parameters in terms of moments we need to solve the set of nonlinear Eqs. (23a)–(23e).

First, combining Eqs. (23a), (23d), (23b), and (23e), we determine the parameters $\hat{p}_u$ and $\hat{p}_h$ in terms of the skewnesses of vertical velocity and temperature, and the parameter p_S. The result is

$$
\hat{p}_u = \frac{1}{2} \left(1 - \frac{\langle S \rangle_w}{\sqrt{4/p_S + \langle S \rangle_w^2}} \right) = \frac{\langle S_- \rangle_w}{\langle S_+ \rangle_w + \langle S_- \rangle_w},
\tag{26a}
$$

$$
\hat{p}_h = \frac{1}{2} \left(1 - \frac{\langle S \rangle_\theta}{\sqrt{4/p_S + \langle S \rangle_\theta^2}} \right) = \frac{\langle S_- \rangle_\theta}{\langle S_+ \rangle_\theta + \langle S_- \rangle_\theta},
\tag{26b}
$$

with

$$\langle S_{\pm}\rangle_{\phi} = \frac{1}{2}\left(\sqrt{4/p_S + \langle S\rangle_{\phi}^2} \pm \langle S\rangle_{\phi}\right), \quad \phi = [w, \theta] \cdot \quad (27)$$

The complementary conditional probabilities $\hat{p}_d$ and $\hat{p}_c$ follow from the normalization condition. They are expressed by Eqs. (26a) and (26b), where the sign minus is replaced by plus in the first equality, and the skewnesses $\langle S_{\pm}\rangle$ are replaced by $\langle S_{\mp}\rangle$ in the second equality.

Second, using Eqs. (23a) and (23b), we determine the widths of the vertical velocity Δ_w and temperature Δ_θ in terms of their respective variances $\langle w'^2\rangle$ and $\langle \theta'^2\rangle$ and the already known parameters $\hat{p}_u$ and $\hat{p}_h$. Then, expressing $\hat{p}_u$ and $\hat{p}_h$ by Eqs. (26a) and (26b), we find that

$$\Delta_{\phi} = \left(\langle S_+\rangle_{\phi} + \langle S_-\rangle_{\phi}\right)\langle \phi'^2\rangle^{1/2}, \quad \phi = (w, \theta). \quad (28)$$

The widths Δ_w and Δ_θ are proportional to the corresponding variances with the proportionality factors nonlinearly depending on the skewnesses S_w and S_θ. Equation (18) also shows

$$w_u = \langle S_+\rangle_w\langle w'^2\rangle^{1/2}, \quad w_d = -\langle S_-\rangle_w\langle w'^2\rangle^{1/2}. \quad (29)$$

Both w_u and w_d are proportional to the variance of the vertical velocity with the coefficient of proportionality equal to the $\langle S_{\pm}\rangle_w$ functions. This also explains the physical meaning of the $\langle S_{\pm}\rangle_w$ functions as positions of updraft and downdraft normalized by the variance. Analogous expressions also hold for θ_h and θ_c.

Finally, we find the parameter $\hat{p}_{uh}$ in terms of the correlation coefficient $C_{w\theta}$ and the already known parameters $\hat{p}_u$ and $\hat{p}_h$. To this end we solve Eq. (23c) with respect to $\hat{p}_{uh}$ and substitute the expressions for widths. We get

$$\hat{p}_{uh} = \frac{1}{p_S}\frac{\langle w'\theta'\rangle}{\Delta_w\Delta_\theta} + \hat{p}_u\hat{p}_h. \quad (30a)$$

The other three probabilities follow using the relationships (14) and (12):

$$\hat{p}_{uc} = \hat{p}_u - \hat{p}_{uh}, \quad (30b)$$

$$\hat{p}_{dh} = \hat{p}_h - \hat{p}_{uh}, \quad (30c)$$

$$\hat{p}_{dc} = 1 - \hat{p}_{uh} - \hat{p}_{uc} - \hat{p}_{dh}. \quad (30d)$$

All the probabilities (30a)–(30d) can be expressed in terms of the correlation coefficient $\langle C\rangle_{w\theta}$ and skewnesses by using Eqs. (26a), (26b), and (28). The results read as

$$\hat{p}_{uh} = \frac{\langle S_-\rangle_w\langle S_-\rangle_\theta + \left(\frac{1}{p_S}\right)\langle C\rangle_{w\theta}}{(\langle S_+\rangle_w + \langle S_-\rangle_w)(\langle S_+\rangle_\theta + \langle S_-\rangle_\theta)}, \quad (31a)$$

$$\hat{p}_{uc} = \frac{\langle S_-\rangle_w\langle S_+\rangle_\theta - \left(\frac{1}{p_S}\right)\langle C\rangle_{w\theta}}{(\langle S_+\rangle_w + \langle S_-\rangle_w)(\langle S_+\rangle_\theta + \langle S_-\rangle_\theta)}, \quad (31b)$$

$$\hat{p}_{dh} = \frac{\langle S_+\rangle_w\langle S_-\rangle_\theta - \left(\frac{1}{p_S}\right)\langle C\rangle_{w\theta}}{(\langle S_+\rangle_w + \langle S_-\rangle_w)(\langle S_+\rangle_\theta + \langle S_-\rangle_\theta)}, \quad (31c)$$

$$\hat{p}_{dc} = \frac{\langle S_+\rangle_w\langle S_+\rangle_\theta + \left(\frac{1}{p_S}\right)\langle C\rangle_{w\theta}}{(\langle S_+\rangle_w + \langle S_-\rangle_w)(\langle S_+\rangle_\theta + \langle S_-\rangle_\theta)}. \quad (31d)$$

The new feature here is that the individual probabilities (area coverages) (31a)–(31d) depend on not only the skewnesses, as in univariate and conventional trivariate bi-Gaussian models, but on the correlation coefficients as well. The PDF used by Larson and Golaz (2005) and Mironov and Machulskaya (2017) do not contain the correlation coefficient between scalars and vertical velocity, although they account for the correlation between temperature and humidity. The reason is that in the conventional models $\hat{p}_u$ and $\hat{p}_d$ are defined as in univariate models by equations similar to (26a), while the correlation coefficients are attributed to a shape of PDF only.

Summarizing, all the parameters of the bivariate PDF (11) are determined in terms of the 5 lowest-order moments: $\langle w'^2\rangle$, $\langle \theta'^2\rangle$, $\langle w'\theta'\rangle$, $\langle w'^3\rangle$, and $\langle \theta'^3\rangle$, and the parameter p_S.

c. Calculation of closure for bivariate HOMs

All bivariate HOMs are obtained by using Eqs. (26a), (26b), (28), and (30a)–(31d) in Eq. (22). The result of the calculations is

$$\langle w'^n\theta'^m\rangle = \langle C\rangle_{w^n\theta^m}\langle w'^2\rangle^{n/2}\langle \theta'^2\rangle^{m/2}$$

$$= \left[\frac{1}{p_S}A_{n-1m-1} + A_{nm}\langle C\rangle_{w\theta}\right]\langle w'^2\rangle^{n/2}\langle \theta'^2\rangle^{m/2}, \quad (32)$$

where $\langle C\rangle_{w^n\theta^m}$ are the normalized moments (also often called generalized correlation coefficients, or generalized skewnesses),

$$A_{nm} = A_nA_m, \quad A_a = \frac{\langle S_+\rangle_{\phi}^a + (-1)^{a-1}\langle S_-\rangle_{\phi}^a}{\langle S_+\rangle_{\phi} + \langle S_-\rangle_{\phi}}, \quad (33)$$

where $a = [n, m]$, $\phi = [w, \theta]$, $A_{-1} = p_S$, $A_0 = 0$ and $\langle S_{\pm}\rangle$ are defined by Eq. (27).

The predicted TOMs [$n = 2$, $m = 1$ and $n = 1$, $m = 2$ in Eq. (32)] are as follows:

$$\langle C\rangle_{w^2\theta} = \langle S\rangle_w\langle C\rangle_{w\theta}, \quad \langle C\rangle_{w\theta^2} = \langle S\rangle_\theta\langle C\rangle_{w\theta}. \quad (34)$$

The first Eq. (34) describes the flux of heat flux, and the second one the flux of temperature variance. Both fluxes $\langle w'^2\theta'\rangle$ and $\langle w'\theta'^2\rangle$ are responsible for the nonlocal transport. According to Eqs. (34) these TOMs do not dependent of p_S explicitly, but only implicitly via the dependence of the skewness on p_S, see Eqs. (25a) and (25b). It is in contrast to the other bivariate moments, see, e.g., equations for FOMs (35a) to (35e). It is an unexpected result, implying that the TOMs would be the same for flows possessing the same skewness and the heat flux. Moreover, the result shows that the same fluxes exist for closely packed and for dilute distributions of plumes in a convective flow.

Similarly, the FOMs are

$$\langle C\rangle_{w^4} = \frac{1}{p_S} + \langle S\rangle_w^2, \tag{35a}$$

$$\langle C\rangle_{w^3\theta} = \left(\frac{1}{p_S} + \langle S\rangle_w^2\right)\langle C\rangle_{w\theta}, \tag{35b}$$

$$\langle C\rangle_{w^2\theta^2} = \frac{1}{p_S} + \langle S\rangle_w\langle S\rangle_\theta\langle C\rangle_{w\theta}, \tag{35c}$$

$$\langle C\rangle_{w\theta^3} = \left(\frac{1}{p_S} + \langle S\rangle_\theta^2\right)\langle C\rangle_{w\theta}, \tag{35d}$$

$$\langle C\rangle_{\theta^4} = \frac{1}{p_S} + \langle S\rangle_\theta^2. \tag{35e}$$

The FOM $\langle w'^4\rangle$ can be considered as the vertical flux $\langle w'w'^3\rangle$ of the asymmetric fluctuations w'^3. Since this flux is positive, the vertical transport of asymmetric fluctuations must be always upward. The moments (35a), (35b), (35d), and (35e) become Gaussian $\langle w'^4\rangle = 3\langle w'^2\rangle^2$, $\langle w'^3\theta'\rangle = 3\langle w'^2\rangle\langle w'\theta'\rangle$, $\langle w'^3\theta'\rangle = 3\langle\theta'^2\rangle\langle w'\theta'\rangle$, and $\langle\theta'^4\rangle = 3\langle\theta'^2\rangle^2$ for $p_S = 1/3$ and $\langle S\rangle_w = 0$, $\langle S\rangle_\theta = 0$.

Although the TOMs (34) are independent of p_S, this does not mean that all odd-order moments are independent of p_S too. An example of the fifth-order moment $\langle w'^5\rangle$ ($n = 5$, $m = 0$) is as follows:

$$\langle C\rangle_{w^5} = \langle S\rangle_w\left(\frac{2}{p_S} + \langle S\rangle_w^2\right). \tag{36}$$

The closure (36) demonstrates the opposite, as well as the similar formula for $\langle\theta'^5\rangle$. In the limit of unskewed turbulence $\langle w'^5\rangle = \langle\theta'^5\rangle = 0$ for all values of p_S. For the Gaussian turbulence $\langle w'^5\rangle = \langle\theta'^5\rangle = 0$ also, because these are odd-order moments.

For further increasing order of the moments, e.g., to sixth order with $n = 6$, $m = 0$, we obtain the closure as

$$\langle C\rangle_{w^6} = \frac{1}{p_S^2} + \langle S\rangle_w^2\left(\frac{3}{p_S} + \langle S\rangle_w^2\right). \tag{37}$$

Equation (37) shows that for $p_S = 1/3$ in the unskewed limit $\langle w'^6\rangle = 9\langle w'^2\rangle^3$, while for the corresponding Gaussian moment $\langle w'^6\rangle = 15\langle w'^2\rangle^3$. Thus, while for $p_S = 1/3$ the FOMs and the fifth-order moments are Gaussian in the unskewed turbulence limit, all further HOMs are non-Gaussian. This moment demonstrates the correlation of asymmetric fluctuations w'^3, since $w'^6 = w'^3w'^3$ from one hand side, and of symmetric fluctuations w'^2 and w'^4, since $w'^6 = w'^2w'^4$ from the other side. Similarly for θ'^6.

Finally, we derive the bivariate HOM $\langle w'\theta'^4\rangle$ ($n = 1$, $m = 4$), which is important for discussion of advanced closure models (see section 8). This moment describes the nonlocal transport of $\langle\theta'^4\rangle$ and is given as

$$\langle C\rangle_{w\theta^4} = \langle S\rangle_\theta\left(\frac{2}{p_S} + \langle S\rangle_\theta^2\right)C_{w\theta}. \tag{38}$$

This flux becomes zero for unskewed turbulence, i.e., if $\langle S\rangle_w \to 0$. For the Gaussian turbulence $\langle w'\theta'^4\rangle = 0$ also.

Similar to Eqs. (32) and (33), closures can be calculated for all 5 remaining bivariate PDFs, see Table 1. For each pair of variables one can easily obtain all of them by applying relabeling symmetry to the above-mentioned Eqs. (32) and (33). As an example, we consider $\langle w'^n u'^k\rangle$, which describes features related to the vertical transport of the along-wind fluctuations. In this case the explicit formulas are given by Eqs. (32) and (33), where the variable θ is replaced by u. Thus, we obtain, e.g., for $\langle w'^2 u'\rangle$ and $\langle w'u'^2\rangle$, the closure equations as $\langle C\rangle_{w^2u} = \langle S\rangle_w\langle C\rangle_{wu}$ and $\langle C\rangle_{wu^2} = \langle S\rangle_u\langle C\rangle_{wu}$. These equations are very similar to Eqs. (34). However, this similarity of the functional form of the closures does not imply a similarity of the momentum and heat transfer in the convective boundary layer.

6. Trivariate closures for HOMs

The trivariate 9-delta-PDF $P(w', \theta', u')$ depends on 15 parameters, correspondingly the closure equations for HOMs are defined by 10 irreducible moments and p_S as a parameter. Similarly to Eqs. (32) and (33) the closures for the trivariate HOMs are calculated following the solution guide reported in section 3.

We chose as irreducible moments

$$\begin{aligned}&\langle w'^2\rangle, \langle\theta'^2\rangle, \langle u'^2\rangle, \langle w'\theta'\rangle, \langle w'u'\rangle, \langle\theta'u'\rangle,\\&\langle w'^3\rangle, \langle\theta'^3\rangle, \langle u'^3\rangle, \langle w'\theta'u'\rangle.\end{aligned} \tag{39}$$

These include all SOMs, all univariate TOMs, and one moment describing triple correlation of the lowest order. All the other HOMs are predicted using the moments (39) and parameter p_S.

The result of the straightforward but lengthy calculations (outlined in appendix A) reads

$$\langle w'^n \theta'^m u'^l\rangle = \langle C\rangle_{w^n\theta^m u^l}\langle w'^2\rangle^{n/2}\langle\theta'^2\rangle^{m/2}\langle u'^2\rangle^{l/2}$$

$$= \left[\frac{1}{p_S^2}A_{n-1m-1l-1} + \frac{1}{p_S}\Big(A_{nml-1}\langle C\rangle_{w\theta}\right.$$

$$+ A_{nm-1l}\langle C\rangle_{wu} + A_{n-1ml}\langle C\rangle_{\theta u}\Big)$$

$$\left.+ A_{nml}\langle C\rangle_{w\theta u}\right]\langle w'^2\rangle^{n/2}\langle\theta'^2\rangle^{m/2}\langle u'^2\rangle^{l/2}, \tag{40}$$

where $A_{nml} = A_nA_mA_l$, $A_a(S_\phi)$, and $S_{\phi\pm}(p_S)$ are defined as before by Eqs. (33) and (27) with $a = [n, m, l]$ and $\phi = [w, \theta, u]$. The final formulas (40) have a functional form that is an inductive extension of that of the bivariate Eqs. (32).

Several trivariate FOMs are of special interest, these are the moments that present the transport terms of dynamic equations for irreducible TOMs, e.g., $\langle w'^2\theta'u'\rangle$ describing a vertical transport of $\langle w'\theta'u'\rangle$. Using $n = 2$ and $m = l = 1$ in Eq. (40) we obtain the following explicit expressions:

$$\langle C\rangle_{w^2\theta u} = \frac{1}{p_S}\langle C\rangle_{\theta u} + \langle S\rangle_w\langle C\rangle_{w\theta u}. \qquad (41a)$$

In contrast to the transport of heat flux and variances [Eq. (34)], the transport of trivariate moment $\langle w'\theta'u'\rangle$ depends on the background (parameter p_S). This moment is non-Gaussian in the limit of $\langle S\rangle_w \to 0$ (the Gaussian reads $\langle w'^2\theta'u'\rangle = \langle w'^2\rangle\langle\theta'u'\rangle + 2\langle w'\theta'\rangle\langle w'u'\rangle$). The other two trivariate FOMs $\langle w'\theta'^2u'\rangle$ and $\langle w'\theta'u'^2\rangle$ are given by formulas similar to (41a). Thus the closure describing the correlations of vertical $w'\theta'$ and horizontal $u'\theta'$ fluctuations of heat flux reads as

$$\langle C\rangle_{w\theta^2 u} = \frac{1}{p_S}\langle C\rangle_{wu} + \langle S\rangle_\theta\langle C\rangle_{w\theta u}, \qquad (41b)$$

and the closure for correlations of vertical heat flux $w'\theta'$ and horizontal variance u'^2 fluctuations as

$$\langle C\rangle_{w\theta u^2} = \frac{1}{p_S}\langle C\rangle_{w\theta} + \langle S\rangle_u\langle C\rangle_{w\theta u}. \qquad (41c)$$

They are non-Gaussian as well.

As explained in the section 3, see also Table 1, there are four families of trivariate moments $\langle w'^n\theta'^mu'^l\rangle$, $\langle w'^n\theta'^m\upsilon'^k\rangle$, $\langle w'^nu'^l\upsilon'^k\rangle$, and $\langle\theta'^mu'^l\upsilon'^k\rangle$. An extension to all trivariate complementary closures is similar to this for bivariate closures. Thus the closures describing the vertical transport of trivariate moment $\langle w'\theta'\upsilon'\rangle$ can be easily obtained using relabeling symmetry in Eq. (41a). The result reads as

$$\langle C\rangle_{w^2\theta\upsilon} = \frac{1}{p_S}\langle C\rangle_{\theta\upsilon} + \langle S\rangle_w\langle C\rangle_{w\theta\upsilon}. \qquad (42)$$

7. Quadrivariate closures for HOMs

For the general 17-delta-PDF (5) the following 19 moments are the irreducible ones:

$$\begin{aligned}
&\langle w'^2\rangle, \langle\theta'^2\rangle, \langle u'^2\rangle, \langle\upsilon'^2\rangle, \\
&\langle w'\theta'\rangle, \langle w'u'\rangle, \langle w'\upsilon'\rangle, \langle\theta'u'\rangle, \langle\theta'\upsilon'\rangle, \langle u'\upsilon'\rangle, \\
&\langle w'^3\rangle, \langle\theta'^3\rangle, \langle u'^3\rangle, \langle\upsilon'^3\rangle, \\
&\langle w'\theta'u'\rangle, \langle w'\theta'\upsilon'\rangle, \langle w'u'\upsilon'\rangle, \langle\theta'u'\upsilon'\rangle, \\
&\langle w'\theta'u'\upsilon'\rangle.
\end{aligned} \qquad (43)$$

Here all SOMs and the four univariate TOMs are chosen as irreducible moments. The other six TOMs are predicted. All four trivariate moments describing triple correlation of the lowest order are used. The only quadrivariate moment $\langle w'\theta'u'\upsilon'\rangle$ is chosen to combine all independent variables. All other HOMs are predicted in terms of the moments (43) and parameter p_S.

The final closure equations can be written in a functional form that is an inductive extension of that of the bivariate and trivariate equations [(32) and (40), respectively]. The result reads

$$\langle w'^n\theta'^mu'^l\upsilon'^k\rangle = \langle C\rangle_{w^n\theta^mu^l\upsilon^k}\langle w'^2\rangle^{n/2}\langle\theta'^2\rangle^{m/2}\langle u'^2\rangle^{l/2}\langle\upsilon'^2\rangle^{k/2}$$

$$\begin{aligned}
= \Bigg[&\frac{1}{p_S^3}A_{n-1m-1l-1k-1} + \frac{1}{p_S^2}\big(A_{nml-1k-1}\langle C\rangle_{w\theta} \\
&+ A_{nm-1lk-1}\langle C\rangle_{wu} + A_{nm-1l-1k}\langle C\rangle_{w\upsilon} \\
&+ A_{n-1mlk-1}\langle C\rangle_{\theta u} + A_{n-1ml-1k}\langle C\rangle_{\theta\upsilon} \\
&+ A_{n-1m-1lk}\langle C\rangle_{u\upsilon}\big), + \frac{1}{p_S}\big(A_{nmlk-1}\langle C\rangle_{w\theta u} \\
&+ A_{nml-1k}\langle C\rangle_{w\theta\upsilon} + A_{nm-1lk}\langle C\rangle_{wu\upsilon} \\
&+ A_{n-1mlk}\langle C\rangle_{\theta u\upsilon}\big) + A_{nmlk}\langle C\rangle_{w\theta u\upsilon}\Bigg] \\
&\times \langle w'^2\rangle^{n/2}\langle\theta'^2\rangle^{m/2}\langle u'^2\rangle^{l/2}\langle\upsilon'^2\rangle^{k/2}, \qquad (44)
\end{aligned}$$

where $A_{nmlk} = A_nA_mA_lA_k$, and $A_a(S_\phi)$ with $a = [n, m, l, k]$ is given by Eq. (33) and $S_{\phi\pm}$ with $\phi = [w, \theta, u, \upsilon]$ is defined by Eqs. (27). The intermediate calculations are given in appendix B.

Although the moments provided by Eqs. (44) obey the same universal functional form as bivariate and trivariate moments, a new feature exists: it is the presence of one more new object, the correlation coefficient $\langle C\rangle_{w\theta u\upsilon}$ relating all four variables.

Equations (44) give the following explicit expressions for the lowest-order ($n = 2, m = l = k = 1$) quadrivariate HOM:

$$\langle C\rangle_{w^2\theta u\upsilon} = \langle S\rangle_w\langle C\rangle_{w\theta u\upsilon}. \qquad (45)$$

There are four such moments that are quadratic in one of the variables. For the other variables the closures are similar to Eq. (45). The quadrivariate HOM $\langle w'^2\theta'u'\upsilon'\rangle$ describes the transport of the irreducible FOM $\langle w'\theta'u'\upsilon'\rangle$ in dynamic closure models. For $\langle S\rangle_w = 0$ we have $\langle w'^2\theta'u'\upsilon'\rangle = 0$, as for the corresponding Gaussian moment. The other moments also describe the correlations of any variable w', θ', u', and υ' with quadrivariate fluctuations $w'\theta'u'\upsilon'$ defining the irreducible moment $\langle w'\theta'u'\upsilon'\rangle$. Similarly to TOMs (34), but contrary to trivariate moments (41a), these four moments do not depend on the background (parameter p_S). Thus the moments remain unchanged for regimes with dense packing of plumes ($p_S \sim 1$) and for those of dilute packing ($p_S \to 0$). The other quadrivariate HOMs can be derived similarly.

The quadrivariate closure Eqs. (44) complete the solution of the closure problem for 17-delta-PDF (5) when the parameter p_S is specified.

8. Specification of parameter p_S and analytical ADAMs

The choice of the parameter p_S is not unique. We consider several hypotheses, which result in several assumed delta-PDF approximation closure models (ADAMs). Probably the most straightforward approach is to determine p_S by using one more irreducible moment. Since the predicted TOMs do not depend of p_S [see Eqs. (34)], they cannot be used for this purpose. And since p_S is a scalar we prefer a moment based on a scalar. There is only one such fourth-order moment: θ'^4.

Taking the closure for $\langle \theta'^4 \rangle$, the equation defining the parameter p_S follows from Eq. (35e) as

$$p_S = \frac{1}{\langle C \rangle_{\theta^4} - \langle S \rangle_\theta^2}, \tag{46}$$

where $\langle C \rangle_{\theta^4}$ is the kurtosis in temperature. Substituting Eq. (46) in Eq. (44) one can obtain a completely closed model. However, the analysis of the resulting closure equations reveals that such closure model has a drawback. Namely, substitution of Eq. (46) in Eq. (35a), and similar for all the other variables, shows a separation of variables as

$$\langle C \rangle_{\theta^4} - \langle S \rangle_\theta^2 = \langle C \rangle_{w^4} - \langle S \rangle_w^2 = \langle C \rangle_{u^4} - \langle S \rangle_u^2 = \langle C \rangle_{v^4} - \langle S \rangle_v^2$$
$$= \frac{1}{p_S}. \tag{47}$$

This equation is satisfied trivially when $\langle C \rangle_{\theta^4} = \langle C \rangle_{w^4} = \langle C \rangle_{u^4} = \langle C \rangle_{v^4}$ and $\langle S \rangle_\theta = \langle S \rangle_w = \langle S \rangle_u = \langle S \rangle_v$. Thus the solution (46) is well suited only for the univariate limit of PDF (5), but not in the general case.

a. ADAM/P_S

A more general solution, which fulfills Eq. (47), suggests that p_S should not depend on a moment at all, i.e.,

$$p_S = \text{const}, \quad 0 < p_S \leq 1. \tag{48}$$

The solution is not unique. Any constant in the range $0 < p_S \leq 1$ can be used. This leads to an analytical ADAM/PS, where the abbreviation PS means that the probability of structures is chosen according to Eq. (48).

An approach that allows a specification of the value of the constant p_S would be to apply some correspondence principle:

b. ADAM/QN

For consistency of ADAMs with the HOM closure models using quasi normality of FOMS (Millionshchikov hypothesis) one can propose p_S as a constant

$$p_S = \frac{1}{3}. \tag{49}$$

Thus, after substituting Eq. (49) in Eq. (44), the model ADAM/QN follows. QN in the abbreviation means the Gaussian limit of FOMs.

In particular, substituting Eq. (49) in Eqs. (35a)–(35e) we get the closure Eqs. (4a), (4b), (4d), (4e) based on the universality hypothesis of GH02 and GH05. Nevertheless, a conceptual difference exists in the treatment of the closures of GH02 and GH05 and the new closure model ADAM/QN. The former are derived using additionally a linear interpolation assumption, while the latter are obtained as exact solution of the closure Eq. (44). In this respect the universality hypothesis of GH02 and GH05 [Eqs. (4a)–(4e) and similar ones for other variables] is proven now, using ADAM/QN, for all FOMs with exception of the moment (4c) and similar ones for other variables. In ADAM/QN the latter moments are replaced by the moment (35c) and analogously for other variables.

c. ADAM/MF

For correspondence with the mass-flux theories one can use

$$p_S = 1, \tag{50}$$

that is, we have no background turbulent motion [$p_0 = 0$, see Eq. (6a)]. This leads to one more closure model ADAM/MF (MF means mass flux), after substituting Eq. (50) in Eq. (44). The ADAM/MF provides an extension of the traditional mass-flux closures to multivariate HOMs.

Summarizing, the closure problem for the 17-delta-PDF (5) is solved completely. The general quadrivariate ADAMs include 6 bivariate and 4 trivariate submodels of lower levels of complexity, see Table 1. The solution is not unique, as it should be for any closure problem. But we stress that all solutions are derived without any ad hoc simplifying assumptions. All closures have correct physical dimensions, respects symmetries, including sign changes of variables and relabeling. For all choices of closure for the parameter p_S, as long as p_S remains in the range $0 < p_S \leq 1$, the resulting closures for HOMs are realizable closures, because they are derived using the same PDF.

The testing of closures assumes that a connection of the modeled moments to the moments based on atmospheric measurements, DNS and LES data is established. For the irreducible moments we use the proposition

$$\langle w'^n \theta'^m u'^l v'^k \rangle = \overline{w'^n \theta'^m u'^l v'^k}, \tag{51}$$

where the averaging is defined by the Reynolds rule and by the 17-delta-PDF, as before. Thus, finally, the closure problem for 17-delta-PDF (5) is solved in terms of the Reynolds moments.

9. Background of testing

The fidelity of the new closure equations must be supported by comparison with data from measurements and appropriate numerical simulations (a priori test) or by their implementation in dynamic closure models (a posteriori test). In our a priori test we mostly rely on a comparison with data from field measurements (Hartmann et al. 1999), but also use data from LES (Raasch and Schröter 2001) and DNS (Waggy et al. 2016) simulations. The field data have the advantage of large Reynolds numbers in comparison to DNS and of independence on subgrid closure assumptions in comparison to LES. For a description of the data please refer to the original papers. All data represent a well-developed dry convective turbulent boundary layer as shown in Fig. 3 by a constant wind speed and zero gradient of the potential temperature in the bulk of the mixed layer. In Fig. 3 and most of the following figures we present vertical profiles of the data by applying a locally weighted regression method (lowess) suggested by Cleveland (1979). We show an example in Fig. 4. Lowess combines smoothing and interpolating of scattered data in order to facilitate graphical presentation. For each point x of the output data individual weights are calculated for the input data depending on the distance of their abscissa value from
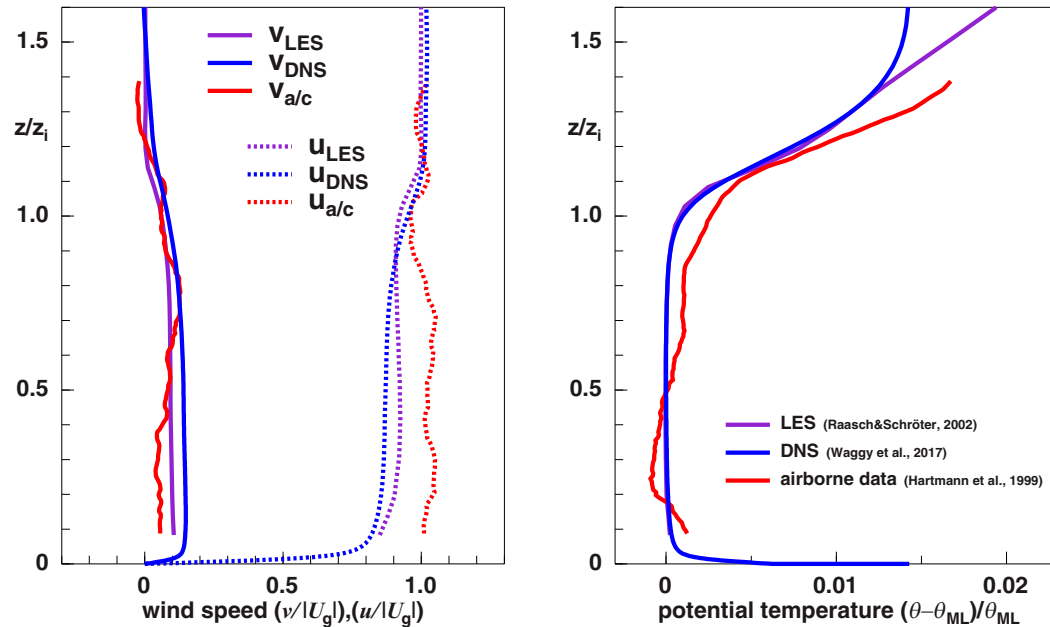
FIG. 3. Vertical profiles of the wind components and of the potential temperature for the measurements (red), the LES (purple), and the DNS (blue) data. The height is normalized by z_i. The airborne profiles represent the average of a descent and subsequent ascent directly after stack I on 5 Apr 1998 (refer to Table I in GH02). (left) The horizontal wind components, with u positive along the mean wind, and v positive to the right of the mean wind; both are normalized by the geostrophic wind speed. The geostrophic wind speed is $U_g = \left(u_g^2 + v_g^2\right)^{1/2} \approx 12\,\mathrm{m\,s^{-1}}$ at $z/z_i > 1.1$. (right) The potential temperature referenced to the mean potential temperature in the middle of the mixed layer. Note that the LES and DNS profiles are averages over the entire domain of the simulations while the aircraft data are instantaneous measurements that contain some turbulent fluctuations.

this x and an individual regression is calculated based on the entire input data field. Lowess is thus an n^2 algorithm and designed for small datasets. We use an inverse distance weighting, the weights are (1/distance), with a limitation to a maximum weight of 10 for small distances. A third-degree polynomial fit is used for the regression function.

For comparison of the statistics we apply Deardorff scaling (Deardorff 1970): w_* for all components of velocities and
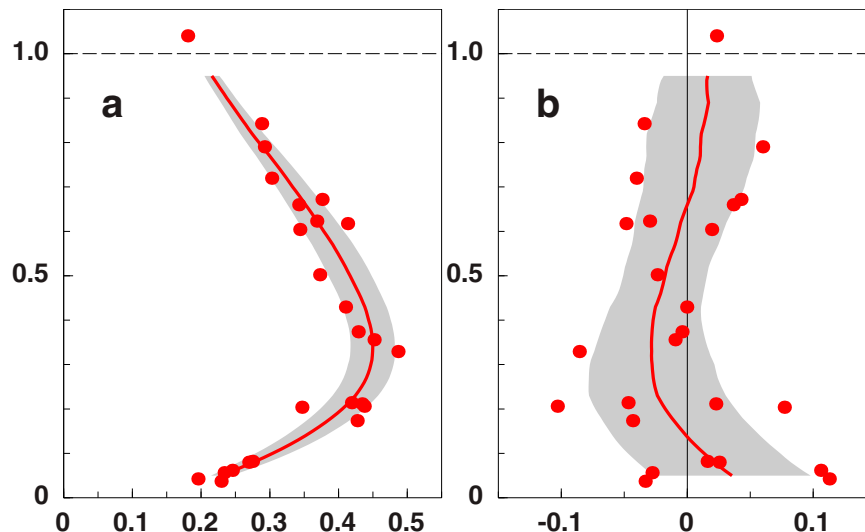

FIG. 4. An example of the lowess procedure applied to present the scattered measurement data. In both graphs the red dots are the normalized measurement data. The red lines show the lowess fits and the gray areas the standard deviation of the data points with respect to their individual lowess fit. (a) $\overline{w^2}$ and (b) $\overline{w\theta v}$.

θ_* for temperature: $w_* = \left(\overline{w'\theta'_0}z_i\right)^{1/3}$, $\theta_* = \left(\overline{w'\theta'_0}\right)^{2/3}/z_i^{1/3}$, where $\overline{w'\theta'_0}$ is the surface value of the heat flux and z_i is the boundary layer height. The quasi-stationary turbulence statistics are quantified by the nondimensional moments $M_{nmlk} = \overline{w'^n\theta'^m u'^l v'^k}/w_*^{n+l+k}\theta_*^m$.

All irreducible moments (51) are shown in Fig. 5. Although there is a significant scatter in some of the aircraft measurements around the LES and DNS profiles, especially in the surface layer, these irreducible moments can be considered as representative for determining the parameters of PDF and for testing of the closures.

10. Testing the parameters of the 17-delta-PDF

With the irreducible moments chosen (43), the 25 parameters of the 17-delta-PDF [Eq. (5)], i.e., the 8 PDF components w_u, w_d, θ_h, θ_c, u_f, u_b, v_r, and v_l can be determined using Eqs. (18) with (19), and (26a) to (30d) for the vertical velocity components and the temperature and in analogy with permutations for the other variables. The 16 probabilities p_{uhfr}, $\ldots$, p_{dcbl} can be obtained using Eqs. (B2)–(B3o) given in appendix B.

Vertical profiles of the delta-PDF components and the individual probabilities are shown in Fig. 6. The profiles of w_u and w_d reflect the decay of $\overline{w'^2}$ near the surface and in the stably stratified inversion above (Fig. 5), as well as the maximum in the middle of mixing zone. In contrast, the profiles of θ_h and θ_c increase near the surface, have maximum in the inversion layer reflecting all the characteristic features of the profile of $\overline{\theta'^2}$ (Fig. 5). In Fig. 6 we also show the profiles of u_f and u_b, which are nearly constant in the middle of the boundary layer, but show a maximum at the surface and a weak increase near the inversion. There the moments of the horizontal velocity components $\overline{u'^2}$ and $\overline{v'^2}$ are largest (see Fig. 5). The large asymmetry in the values of updrafts w_u and downdrafts w_d, and hot θ_h and cold θ_c PDF components can be explained by large skewnesses S_w and S_θ. And vice versa the large skewnesses give rise to the asymmetry of w_u and w_d. The profile of skewnesses for all four variables are shown in Fig. 7. This figure also shows that the skewnesses S_u and S_v are small due to compensations $u_b \approx -u_f$ and $v_l \approx -v_r$.

The profiles of the individual probabilities are not simple as Fig. 6 shows. It is an expected result, because the quadrivariate probabilities are expression in terms of four skewnesses, six bivariate, four trivariate, and one quadrivariate correlation coefficients. But what is most important, none of the probabilities is negative, as it should be. Thus, all moments pass the test on realizability.

11. Predicting and explaining the profiles of HOMs

In this section we present vertical profiles of the moments as predicted by the closure equations and compare them to profiles from measurements, LES and DNS data. Our theory predicts an infinite number of HOMs based on the 19 irreducible moments. We have tested a total of 72 predicted lowest-order moments and present here those moments, which play a key role in HOC RANS models and some further ones that have very nontrivial profiles, in order to assess the strengths and the weakness of the new closure models [see Eqs. (34) to (38) and (41a) to (42)].

The profiles of these HOMs are shown in Fig. 8. We visualize the HOMs for the case of the ADAM/QN, ADAM/MF and for the case of a large background coverage $p_S = 0.2$ ($p_0 = 0.8$). Shaded areas show the range $0.2 \leq p_S \leq 1$. Although the profiles of the predicted HOMs look very complex and different from each other, qualitatively their characteristic features can be understood quite simply.

a. Impact of the area coverage parameter p_S

The impact of parameter p_S on all HOMs is significant, see the shaded areas in Fig. 8. In the range $0.2 < p_S \leq 1$, the absolute values of the moments can vary by a factor of 2–3 or even more. The absolute value of all moments increases with decreasing parameter p_S. A small p_S means a small area coverage of the circulation cells, corresponding to large amplitudes due to the mass conservation constraint. The impact of p_S on moments increases when the order of moments increase, cf. the moments $\overline{w'^3}$, $\overline{w'^5}$ and $\overline{w'^4}$, $\overline{w'^6}$ and similar for temperature.

For several moments, such as $\overline{w'^4}$, $\overline{\theta'^4}$, $\overline{u'^4}$, $\overline{w'\theta'^3}$, and $\overline{w'^2\theta'u'}$, ADAM/QN shows a good agreement of the predicted profiles and corresponding profiles from measurements. For the other moments the agreement is marginal in amplitude, but the shape of profiles is reproduced by ADAM/QN very well, see, e.g., the moments $\overline{w'^3\theta'}$, $\overline{w'^3u'}$, and $\overline{w'^2\theta'v'}$.

However, the ADAM/QN is not acceptable for the description of the moment $\overline{w'^2v'^2}$. The best fitting for this moment gives ADAM/MF, which is based on $p_S = 1$. ADAM/QN and ADAM/MF are unable to describe $\overline{w'^2\theta'^2}$ and $\overline{\theta'^2u'^2}$ at all heights. Only in the middle of the boundary layer the profiles approach those of the measurements.

b. Impact of variances

As predicted by the general closure Eqs. (44), the moments are directly proportional to the variances in the corresponding powers. Moments involving vertical velocity fluctuations are small near the surface and near the inversion and are larger in the middle of the mixed layer just as the vertical velocity variance. Please compare, e.g., the profiles of moments $\overline{w'^4}$, $\overline{w'^6}$, and $\overline{w'^2}$ in Figs. 8 and 5. On the contrast, moments involving fluctuations of temperature and horizontal velocity are large toward the limits of the convection zone and small in the middle of the mixed layer, as temperature and horizontal velocity variances do. Compare, e.g., the profiles of moments $\overline{\theta'^4}$ and $\overline{\theta'^2}$, see Figs. 8 and 5.

However, as stated by the closure equations, Eqs. (44), this explanation is correct only if correlation coefficients and skewnesses are constants in height. This is indeed the case for the HOMs in the horizontal velocity fluctuations, but does not hold for moments in the vertical velocity and temperature, see Fig. 7. Thus, in explaining the profiles we cannot neglect the dependence of the correlation coefficients and skewnesses on height.
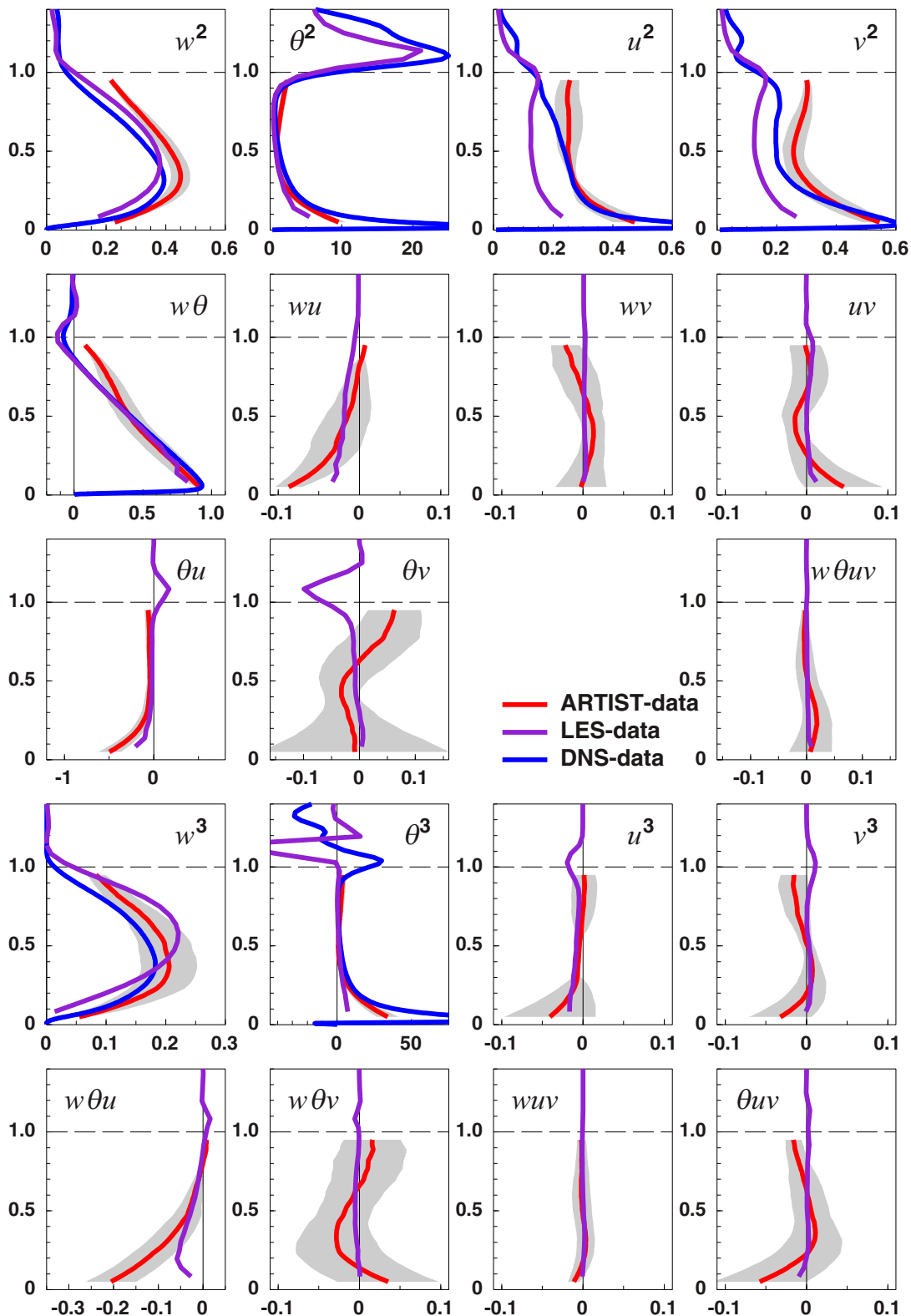
FIG. 5. The 19 irreducible moments used as a base to determine the parameters of the PDF [Eq. (5)]. In this paper the model is fitted to the ARTIST airborne measurements, shown as solid red lines after applying the lowess procedure described in section 9 (cf. Fig. 4). The shaded areas represent the scatter as described in Fig. 4. For comparison, the LES and DNS data (where available) are plotted as purple and blue lines, respectively. Note that several profiles from measurements correspond to those presented in GH02. The essential difference, however, exists as increase of the moments near the surface where the small-scale fluctuations (partly filtered in GH02) are largest.
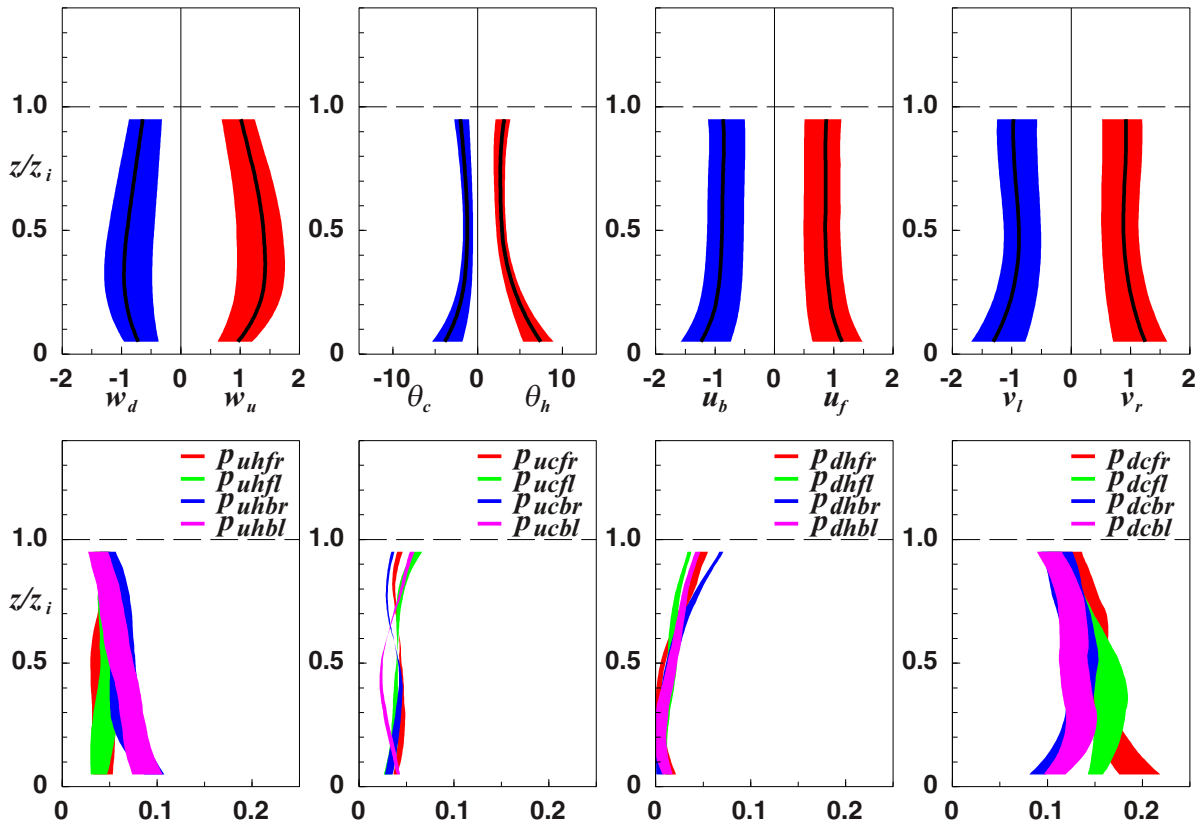
FIG. 6. (top) Vertical profiles of the positions of the delta functions [Eq. (18)]. The blue and red shading mark the range of variation of the values depending on the choice of the parameter p_S for $0.2 < p_S < 1$. The solid black line corresponds to $p_S = 1/3$. The four graphs show (from left to right) w_d, w_u, θ_c, θ_h, u_b, u_f, v_l, and v_r, normalized by w_*. (bottom) Vertical profiles of the 16 probabilities defining the PDF [Eq. (5)] as given by Eqs. (B2)–(B3o) with (A3a)–(A3i), (30a)–(30d), and (26a), (26b), and (27). The probabilities are explained by color coding. The width of the shaded areas corresponds to the range of variation of the values depending on the choice of the parameter p_S for $0.2 < p_S \leq 1$.

c. Impact of the correlation coefficients

The dependence of the HOMs on the correlation coefficients is linear for all moments. The values of moments are larger in regions where the correlations are positive and vice versa. The value of $C_{w\theta}$ is always positive, near the surface and in the mixing layer indicating an upward heat transport. This correlation coefficient decays with height and become negative in the entrainment zone. Thus the moment $\overline{w'^2\theta'}$ and $\overline{w'^3\theta'}$ depending on $C_{w\theta}$ [see Eqs. (34) and (35b)] display this property very well. The moment $\overline{w'^3u'}$ depending on C_{wu} is negative because this coefficients is negative, see Fig. 7. The trivariate moment $\overline{w'^2\theta'u'}$ depending on two correlations coefficients $C_{\theta u}$ and $C_{w\theta u}$ [Eq. (41a)] is negative, because $C_{\theta u}$ is negative, but $C_{w\theta u}$ is small. Thus the triple correlations $w'\theta'u'$ are transported by plumes downward only. The complementary moment $\overline{w'^2\theta'v'}$ [Eq. (42)] changes sign in the middle of the CBL by the similar reason, i.e., because $C_{\theta v}$ changes the sign, but $C_{w\theta v}$ is small. We stress that the moment $\overline{w'^2\theta'v'}$ is extremely small; however, the closure captures the sign change effect. The trivariate moment $\overline{w'\theta'^2u'}$ depending on two correlations coefficients C_{wu} and $C_{w\theta u}$ [Eq. (41b)] is

nearly zero in the upper part of CBL, because both C_{wu} and $C_{w\theta u}$ are small in this region. This shows that correlation of $\overline{\theta'^2}$ and momentum flux $\overline{w'u'}$ are significant only in the lower part of CBL, where it is negative, because C_{wu} is negative. In contrary, the moment $\overline{w'\theta'u'^2}$ [Eq. (41c)] describing the correlation of heat flux and horizontal velocity variance is large and positive, because $C_{w\theta}$ is large and positive near the surface and in the middle part of CBL.

d. Impact of skewness

Further information about the profiles is provided by the skewness. Most transparent for this analysis are the moments C_{w4}, C_{w5}, and C_{w6} because they are polynomials in the skewness only. As shown in Fig. 7, S_w and S_θ are always positive, indicating that hot updrafts dominate. While S_u is negative, indicating that backward fluctuations dominate, but S_v are small. The predicted profiles of HOMs reflect these properties. However, the skewness are nonmonotonic functions of height, so their effect on profiles of HOM depends on height also. The odd moments increase when the skewness increase for positive skewness and decrease for negative, while the even
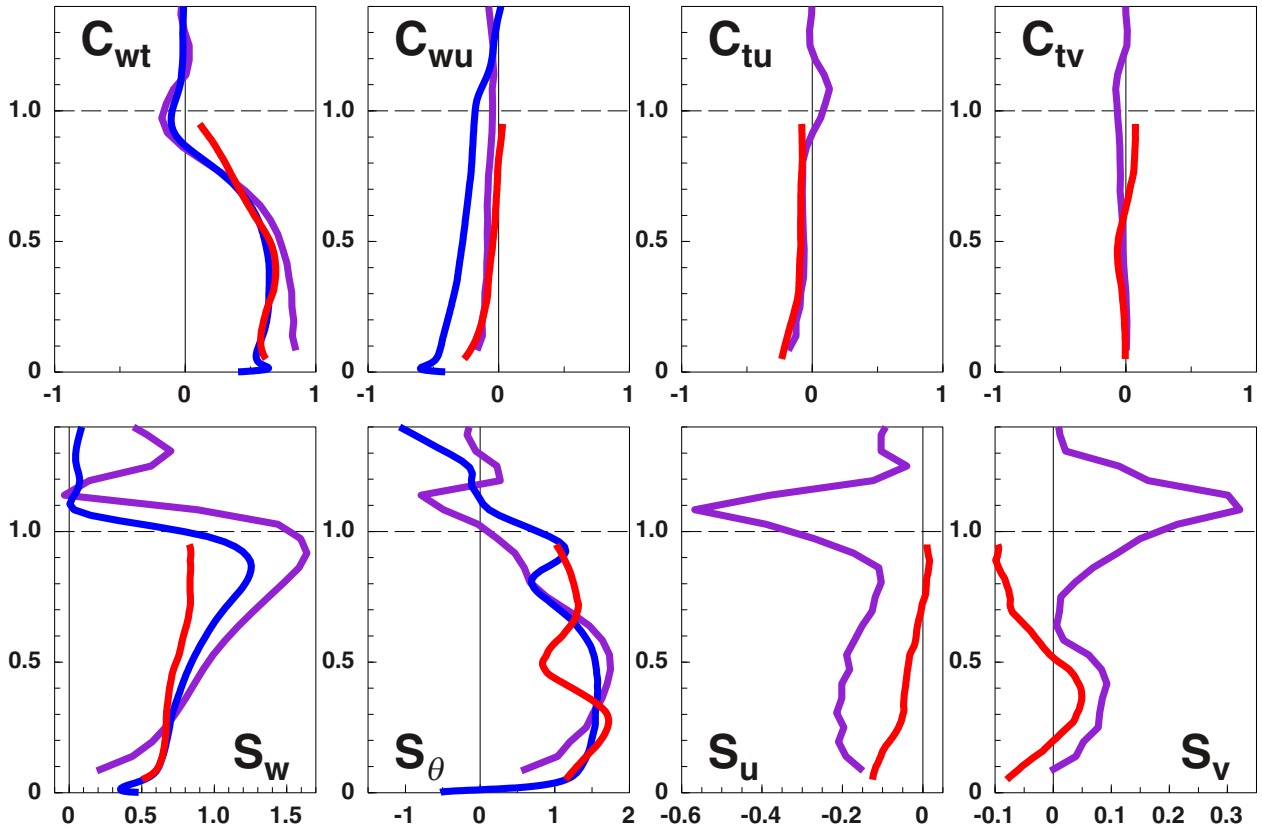
FIG. 7. Profiles of (top, left to right) correlation coefficients $C_{w\theta}$, C_{wu}, $C_{\theta u}$, and $C_{\theta v}$ and (bottom, left to right) skewnesses S_w, S_θ, S_u and S_v, based on the irreducible moments shown in Fig. 5. Red lines are the aircraft measurements, purple lines the LES data, and blue lines the DNS data.

moments always increase with increasing skewnesses, cf. the moments $\overline{w'^4}$ and $\overline{w'^5}$. Only for regions where the skewnesses are small, the profiles of HOMs, e.g., $\overline{u'^4}$, have the structure prescribed by the profiles of variances.

e. Net effect

To show the effects of the individual components (variances, correlation coefficients, skewness, and area coverage parameter) our predicted moments are composed of, we present in Fig. 9 examples of a quantitative analysis of selected bivariate TOMs $\overline{w'^2\theta'}$ and $\overline{w'\theta'^2}$ and univariate FOMs $\overline{w'^4}$ and $\overline{\theta'^4}$. We use the cumulative budget method, which is convenient for analyzing of functions having a multiplicative functional form. In the plots we present by a thin line the variance in temperature in the right-hand side of Eq. (34), a thicker line corresponds to the product of the variances in temperature and in vertical velocity, and so on. The final, most thick line expresses the full moment. In a similar manner we present the monovariate FOM in vertical velocity (35a) and temperature (35e). The only difference is that cumulative budget is used for each term separately, see figure caption for details. The quantitative analysis confirms the validity of the qualitative explanation of the predicted profiles given above. We conclude that all four impacts are important for explanation of the full set of closures for HOMs.

12. Semianalytical ADAMs

Above we have shown that the analytical ADAMs predict the majority of the vertical profiles of HOMs reasonably well, but we cannot expect that they are able to describe the CBL turbulence in its full complexity. One of the obvious possibilities for improvement is the introduction of empirical constants by keeping the functional form of closures unchanged. The ADAMs are flexible for such a generalization. The empirical constants can account for some of the fluctuations of the area coverages (i.e., values of p_S), the subplume (i.e., finite width for delta functions) and interplume (i.e., distribution in positions of delta functions) contributions. A systematic procedure of introducing empirical constants simultaneously in all closure equations is not so obvious. Our proposal consists of two steps:

Step 1: ADAM/S. To account for the subplume and interplume fluctuations we apply the similarity hypothesis

$$\langle w'^n \theta'^m u'^l v'^k \rangle = k_{w^n \theta^m u^l v^k} \overline{w'^n \theta'^m u'^l v'^k} \qquad (52)$$

to the irreducible moments in the general closure Eq. (44). Here the averaging is defined by the Reynolds rule and by the 17-delta-PDF, as before, and $0 < k_{w^n \theta^m u^l v^k} \le 1$ are empirical constants. In the following we call the ADAM that uses the assumption (52) semianalytical ADAM/S (S for similarity). The resulting equations of the general closures for the predicted multivariate HOMs read as
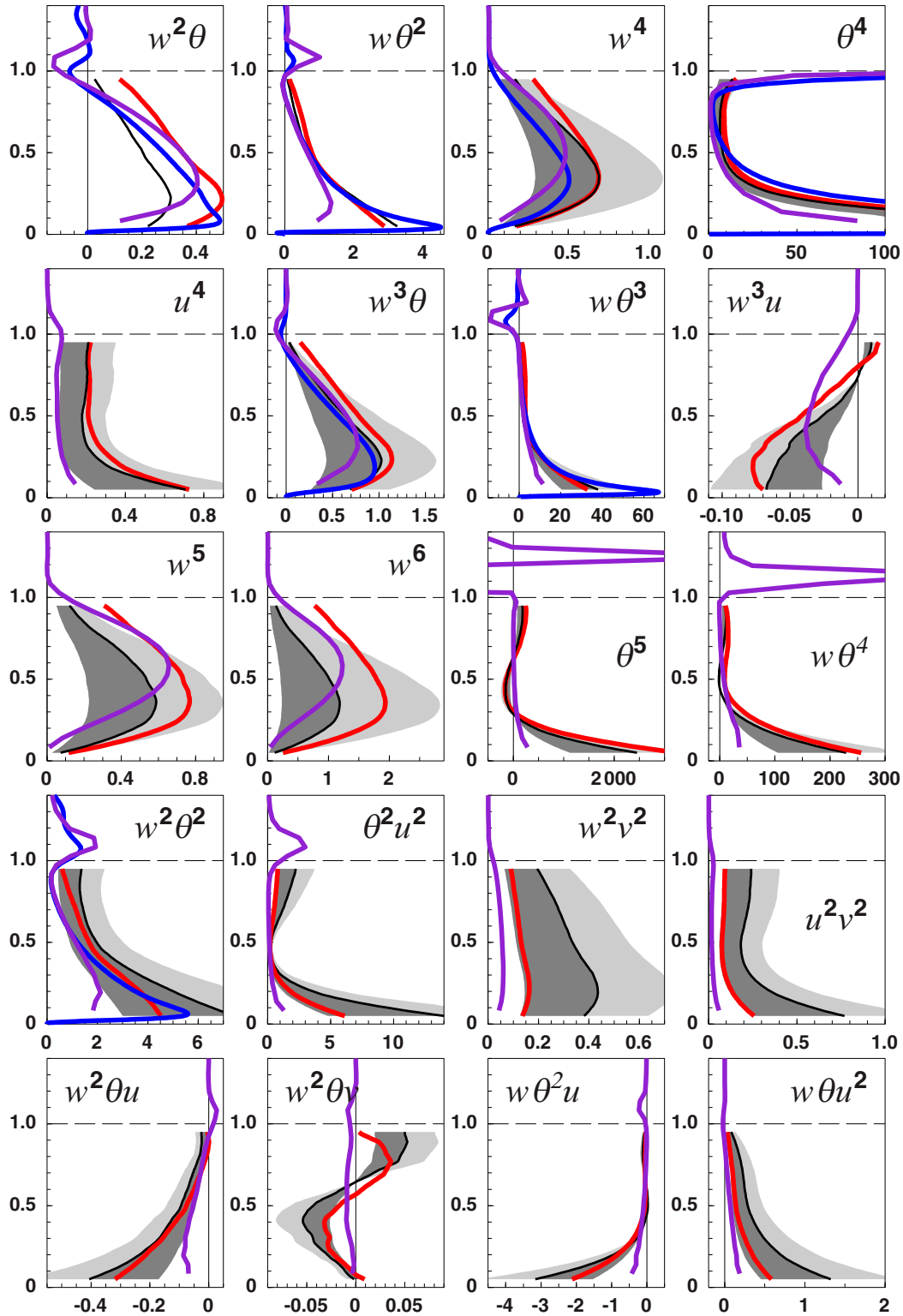
FIG. 8. Predicted HOMs. Red lines are the aircraft measurements, purple lines the LES data and blue lines the DNS. The thin solid black lines are the predicted moments of ADAM/QN based on $p_S = 1/3$. The gray shaded area marks the range of variation of the respective moment with dependence on the parameter p_S for ADAM/PS. Light gray for $0.2 < p_S < 1/3$ and dark gray for $1/3 < p_S \leq 1$. The boundary of dark gray $p_S = 1$ corresponds to ADAM/MF. Note that several profiles from measurements are corresponding to those presented in GH02. The essential difference, however, exists as increase of the moments near the surface where the small-scale fluctuations (partly filtered in GH02) are largest.

$$\overline{w'^n\theta'^m u'^l v'^k} = C_{w^n\theta^m u^l v^k}\overline{w'^2}^{n/2}\overline{\theta'^2}^{m/2}\overline{u'^2}^{l/2}\overline{v'^2}^{k/2}$$

$$= \Bigg[\frac{1}{p_S^3}\frac{k_{w^2}^{n/2}k_{\theta^2}^{m/2}k_{u^2}^{l/2}k_{v^2}^{k/2}}{k_{w^n\theta^m u^l v^k}}A_{n-1m-1k-1l-1}$$

$$+ \frac{1}{p_S^2}\Bigg(k_{w\theta}\frac{k_{w^2}^{n/2-1/2}k_{\theta^2}^{m/2-1/2}k_{u^2}^{l/2}k_{v^2}^{k/2}}{k_{w^n\theta^m u^l v^k}}A_{nml-1k-1}C_{w\theta}$$

$$+ k_{wu}\frac{k_{w^2}^{n/2-1/2}k_{\theta^2}^{m/2}k_{u^2}^{l/2-1/2}k_{v^2}^{k/2}}{k_{w^n\theta^m u^l v^k}}A_{nm-1lk-1}C_{wu}$$

$$+ k_{wv}\frac{k_{w^2}^{n/2-1/2}k_{\theta^2}^{m/2}k_{u^2}^{l/2}k_{v^2}^{k/2-1/2}}{k_{w^n\theta^m u^l v^k}}A_{nm-1l-1k}C_{wv}$$

$$+ k_{\theta u}\frac{k_{w^2}^{n/2}k_{\theta^2}^{m/2-1/2}k_{u^2}^{l/2-1/2}k_{v^2}^{k/2}}{k_{w^n\theta^m u^l v^k}}A_{n-1mlk-1}C_{\theta u}$$

$$+ k_{\theta v}\frac{k_{w^2}^{n/2}k_{\theta^2}^{m/2-1/2}k_{u^2}^{l/2}k_{v^2}^{k/2-1/2}}{k_{w^n\theta^m u^l v^k}}A_{n-1ml-1k}C_{\theta v}$$

$$+ k_{uv}\frac{k_{w^2}^{n/2}k_{\theta^2}^{m/2}k_{u^2}^{l/2-1/2}k_{v^2}^{k/2-1/2}}{k_{w^n\theta^m u^l v^k}}A_{n-1m-1lk}C_{uv}\Bigg)$$

$$+ \frac{1}{p_S}\Bigg(k_{w\theta u}\frac{k_{w^2}^{n/2-1/2}k_{\theta^2}^{m/2-1/2}k_{u^2}^{l/2-1/2}k_{v^2}^{k/2}}{k_{w^n\theta^m u^l v^k}}$$

$$\times A_{nmlk-1}C_{w\theta u}$$

$$+ k_{w\theta v}\frac{k_{w^2}^{n/2-1/2}k_{\theta^2}^{m/2-1/2}k_{u^2}^{l/2}k_{v^2}^{k/2-1/2}}{k_{w^n\theta^m u^l v^k}}A_{nml-1k}C_{w\theta v}$$

$$+ k_{wuv}\frac{k_{w^2}^{n/2-1/2}k_{\theta^2}^{m/2}k_{u^2}^{l/2-1/2}k_{v^2}^{k/2-1/2}}{k_{w^n\theta^m u^l v^k}}A_{nm-1lk}C_{wuv}$$

$$+ k_{\theta uv}\frac{k_{w^2}^{n/2}k_{\theta^2}^{m/2-1/2}k_{u^2}^{l/2-1/2}k_{v^2}^{k/2-1/2}}{k_{w^n\theta^m u^l v^k}}A_{n-1mlk}C_{\theta uv}\Bigg)$$

$$+ k_{w\theta uv}\frac{k_{w^2}^{n/2-1/2}k_{\theta^2}^{m/2-1/2}k_{u^2}^{l/2-1/2}k_{v^2}^{k/2-1/2}}{k_{w^n\theta^m u^l v^k}}$$

$$\times A_{nmlk}C_{w\theta uv}\Bigg]\overline{w'^2}^{n/2}\overline{\theta'^2}^{m/2}\overline{u'^2}^{l/2}\overline{v'^2}^{k/2}, \quad (53)$$

with $A_{nmlk} = A_n A_m A_l A_k$, where $A_a(S_\phi)$ with $a = [n, m, l, k]$ is given by Eq. (33) with $A_{-1} = p_S$, $A_0 = 0$, and $S_{\phi\pm}$ is defined as

$$\langle S_\pm\rangle_\phi = \frac{1}{2}\Bigg(\sqrt{\frac{4}{p_S} + \frac{k_{\phi^3}^2}{k_{\phi^2}^3}S_\phi^2} \pm \frac{k_{\phi^3}}{k_{\phi^2}^{3/2}}S_\phi\Bigg), \quad \phi = [w, \theta, u, v], \quad (54)$$

cf. Eqs. (27).

ADAM/S keeps the functional form of all HOM closures (44), but uses empirical constants $k_{w^n\theta^m u^l v^k}$, their number being equal to the number of irreducible moments. Equations (52) extend the similarity hypothesis for bivariate TOMs
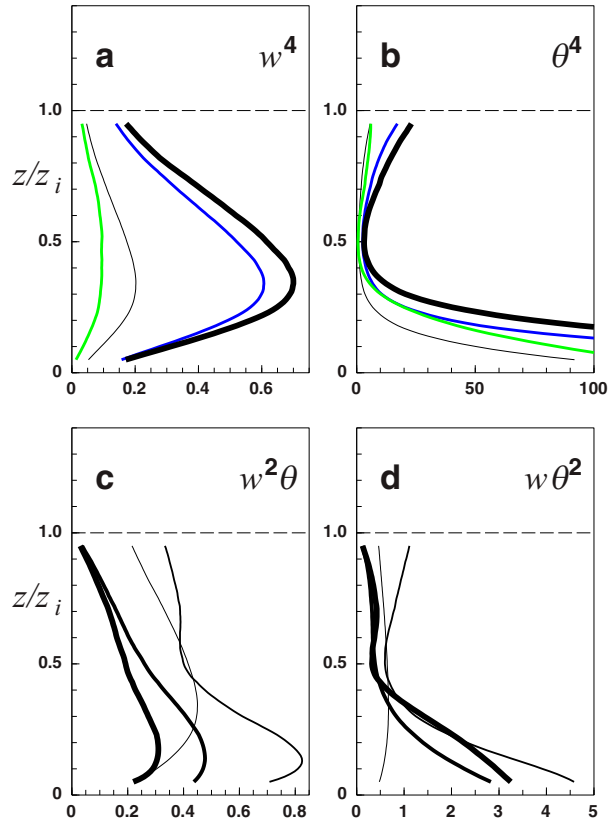

FIG. 9. Illustration of the components of some of the predicted moments. (a) For $\langle w'^4\rangle$ [Eq. (35a)], the thin black line is $\langle w'^2\rangle^2$, the blue line is $\langle w'^2\rangle^2(1/p_S)$, the green line is $\langle w'^2\rangle^2\langle S\rangle_w^2$, and the thick black line is $\langle w'^2\rangle^2(1/p_S) + \langle w'^2\rangle^2\langle S\rangle_w^2$. (b) For $\langle \theta'^4\rangle$ [Eq. (35e)], the thin black line is $\langle \theta'^2\rangle^2$, the blue line is $\langle \theta'^2\rangle^2(1/p_S)$, the green line is $\langle \theta'^2\rangle^2\langle S\rangle_\theta^2$, and the thick black line is $\langle \theta'^2\rangle^2(1/p_S) + \langle \theta'^2\rangle^2\langle S\rangle_\theta^2$. (c) For $\langle w'^2\theta'\rangle$ [Eq. (34)], the lines show, starting from the thinnest with increasing thickness: $\langle w'^2\rangle$, $\langle w'^2\rangle\langle\theta'^2\rangle^{1/2}$, $\langle C\rangle_{w\theta}\langle w'^2\rangle\langle\theta'^2\rangle^{1/2}$, and $\langle S\rangle_w\langle C\rangle_{w\theta}\langle w'^2\rangle\langle\theta'^2\rangle^{1/2}$. (d) For $\langle w'^2\theta'\rangle$ [Eq. (34)], accordingly, $\langle w'^2\rangle$, $\langle w'^2\rangle\langle\theta'^2\rangle^{1/2}$, $\langle C\rangle_{w\theta}\langle w'^2\rangle\langle\theta'^2\rangle^{1/2}$, and $\langle S\rangle_\theta\langle C\rangle_{w\theta}\langle w'^2\rangle\langle\theta'^2\rangle^{1/2}$.

(Abdella and Petersen 2000; Lappen and Randall 2001) and for bivariate FOMs (GH02) to multivariate HOMs. However, the ADAM/S still has deficiencies in the detailed description of convective turbulence. Several predicted moments, e.g., bivariate TOMs $\overline{w'^2\theta'}$ and $\overline{w'\theta'^2}$, which are given by Eqs. (53) with $n = 2, m = 1$, and $k = l = 0$ as

$$\overline{w'^2\theta'} = \frac{k_{w^3}k_{w\theta}}{k_{w^2}^{3/2}k_{w^2\theta}}\left(\frac{\overline{w'^3}}{\overline{w'^2}}\right)\overline{w'\theta'}, \quad (55)$$

cannot distinguish turbulence regimes with dense packing of plumes ($p_S \sim 1$) from those of dilute packing ($p_S \to 0$), because these moments do not depend on p_S. Moreover, the clusters of constants involved in predicted HOM of ADAM/S are mutually dependent, as is apparent from Eqs. (53).

Step 2: ADAM/E. To overcome these limitations of ADAM/S we introduce a further extended similarity hypothesis. This states

that the functional form of the closures remains the same as for ADAM/S, but all clusters of constants in Eq. (53) should be considered as new mutually independent constants. Such a generalization results in a new closure model ADAM/E, where E means extended ADAM.

For example, for Eqs. (55) the extended similarity hypothesis predicts that

$$\overline{w'^2\theta'} = a_{w^2\theta}\left(\frac{\overline{w'^3}}{\overline{w'^2}}\right)\overline{w'\theta'}, \tag{56a}$$

and similarly

$$\overline{w'\theta'^2} = a_{w\theta^2}\left(\frac{\overline{\theta'^3}}{\overline{\theta'^2}}\right)\overline{w'\theta'}, \tag{56b}$$

$$\overline{w'u'^2} = a_{wu^2}\left(\frac{\overline{u'^3}}{\overline{u'^2}}\right)\overline{w'u'}, \tag{56c}$$

where $a_{w^2\theta}$, $a_{w\theta^2}$, and a_{wu^2} are the new empirical constants. We stress that $a_{w^2\theta} \neq k_{w^3}k_{w\theta}/k_{w^2}^{3/2}k_{w^2\theta}$ in general case, and similarly for all the other constants.

We present 17 more closure equations of ADAM/E for the predicted HOMs: the univariate FOMs, generalizing Eqs. (35a) and (35e) and the other bivariate FOMs, which are closely related to the solution of the problem of the refinement of the Millionshchikov hypothesis. These closure equations are as follows:

$$\overline{w'^4} = a_{w^4}\overline{w'^2}^2 + b_{w^4}\left(\frac{\overline{w'^3}}{\overline{w'^2}}\right)^2\overline{w'^2}, \tag{57a}$$

$$\overline{w'^3\theta'} = a_{w^3\theta}\overline{w'\theta'}\,\overline{w'^2} + b_{w^3\theta}\left(\frac{\overline{w'^3}}{\overline{w'^2}}\right)^2\overline{w'\theta'}, \tag{57b}$$

$$\overline{w'^2\theta'^2} = a_{w^2\theta'^2}\overline{w'^2}\,\overline{\theta'^2} + b_{w^2\theta^2}\left(\frac{\overline{w'^3}}{\overline{w'^2}}\right)\left(\frac{\overline{\theta'^3}}{\overline{\theta'^2}}\right)\overline{w'\theta'}, \tag{57c}$$

$$\overline{w'\theta'^3} = a_{w\theta^3}\overline{w'\theta'}\,\overline{\theta'^2} + b_{w^3\theta}\left(\frac{\overline{\theta'^3}}{\overline{\theta'^2}}\right)^2\overline{w'\theta'}, \tag{57d}$$

$$\overline{\theta'^4} = a_{\theta^4}\overline{\theta'^2}^2 + b_{\theta^4}\left(\frac{\overline{\theta'^3}}{\overline{\theta'^2}}\right)^2\overline{\theta'^2}, \tag{57e}$$

$$\overline{u'^4} = a_{u^4}\overline{u'^2}^2 + b_{u^4}\left(\frac{\overline{u'^3}}{\overline{u'^2}}\right)^2\overline{u'^2}, \tag{57f}$$

$$\overline{w'^3u'} = a_{w^3u}\overline{w'u'}\,\overline{w'^2} + b_{w^3u}\left(\frac{\overline{w'^3}}{\overline{w'^2}}\right)^2\overline{w'u'}, \tag{57g}$$

$$\overline{w'^2v'^2} = a_{w^2v^2}\overline{w'^2}\,\overline{v'^2} + b_{w^2v^2}\left(\frac{\overline{w'^3}}{\overline{w'^2}}\right)\left(\frac{\overline{v'^3}}{\overline{v'^2}}\right)\overline{w'v'}, \tag{57h}$$

$$\overline{\theta'^2u'^2} = a_{\theta^2u^2}\overline{u'^2}\,\overline{\theta'^2} + b_{\theta^2u^2}\left(\frac{\overline{\theta'^3}}{\overline{\theta'^2}}\right)\left(\frac{\overline{u'^3}}{\overline{u'^2}}\right)\overline{\theta'u'}, \tag{57i}$$

$$\overline{u'^2v'^2} = a_{u^2v^2}\overline{u'^2}\,\overline{v'^2} + b_{u^2v^2}\left(\frac{\overline{u'^3}}{\overline{u'^2}}\right)\left(\frac{\overline{v'^3}}{\overline{v'^2}}\right)\overline{u'v'}. \tag{57j}$$

The univariate FOMs (57a), (57e), and (57f) attracted much interest recently in relation to the problem of kurtosis–skewness relationships in turbulence. We already addressed this problem in section 5, where we present an extension of the kurtosis–skewness relationships to HOMs, see Eqs. (36) and (37). For this reason we present $\overline{w'^5}$, $\overline{\theta'^5}$, and $\overline{w'^6}$:

$$\overline{w'^5} = a_{w^5}\left(\frac{\overline{w'^3}}{\overline{w'^2}}\right)\overline{w'^2}^2 + b_{w^5}\left(\frac{\overline{w'^3}}{\overline{w'^2}}\right)^3\overline{w'^2}, \tag{58a}$$

$$\overline{\theta'^5} = a_{\theta^5}\left(\frac{\overline{\theta'^3}}{\overline{\theta'^2}}\right)\overline{\theta'^2}^2 + b_{\theta^5}\left(\frac{\overline{\theta'^3}}{\overline{\theta'^2}}\right)^3\overline{\theta'^2}, \tag{58b}$$

$$\overline{w'^6} = a_{w^6}\overline{w'^2}^3 + b_{w^6}\left(\frac{\overline{w'^3}}{\overline{w'^2}}\right)^2\overline{w'^2}^2 + c_{w^6}\left(\frac{\overline{w'^3}}{\overline{w'^2}}\right)^4\overline{w'^2}, \tag{58c}$$

cf. Eqs. (36) and (37).

In addition we also consider the bivariate HOM

$$\overline{w'\theta'^4} = \left[a_{w\theta^4}\overline{\theta'^2} + b_{w\theta^4}\left(\frac{\overline{\theta'^3}}{\overline{\theta'^2}}\right)^2\right]\left(\frac{\overline{\theta'^3}}{\overline{\theta'^2}}\right)\overline{w\theta}, \tag{59}$$

which generalizes Eq. (38).

We provide a generalization of fluxes for triple correlations, which are important for parameterizing the transport terms in HOC RANS models. These closures are given by equations

$$\overline{w'^2\theta'u'} = a_{w^2\theta u}\overline{w'^2}\,\overline{\theta'u'} + b_{w^2\theta u}\left(\frac{\overline{w'^3}}{\overline{w'^2}}\right)\overline{w'\theta'u'}, \tag{60a}$$

$$\overline{w'^2\theta'v'} = a_{w^2\theta v}\overline{w'^2}\,\overline{\theta'v'} + b_{w^2\theta v}\left(\frac{\overline{w'^3}}{\overline{w'^2}}\right)\overline{w'\theta'v'}, \tag{60b}$$

generalizing Eqs. (41a) and (42). Similarly, the generalization of Eqs. (41b) and (41c) leads to closures

$$\overline{w'\theta'^2u'} = a_{w\theta^2u}\overline{\theta'^2}\,\overline{w'u'} + b_{w\theta^2u}\left(\frac{\overline{\theta'^3}}{\overline{\theta'^2}}\right)\overline{w'\theta'u'}, \tag{60c}$$

$$\overline{w'\theta'u'^2} = a_{w\theta u^2}\overline{u'^2}\,\overline{w'\theta'} + b_{w\theta u^2}\left(\frac{\overline{u'^3}}{\overline{u'^2}}\right)\overline{w'\theta'u'}. \tag{60d}$$

In all 20 Eqs. (56a) to (60d) a_{****}, b_{****}, and c_{****} are empirical constants, which we specify in the next step.

13. Specification of empirical constants for the semianalytical ADAM/E

Calculated values of the empirical constants in Eqs. (56a) to (60d) are given in Fig. 10, where we present the best fit to
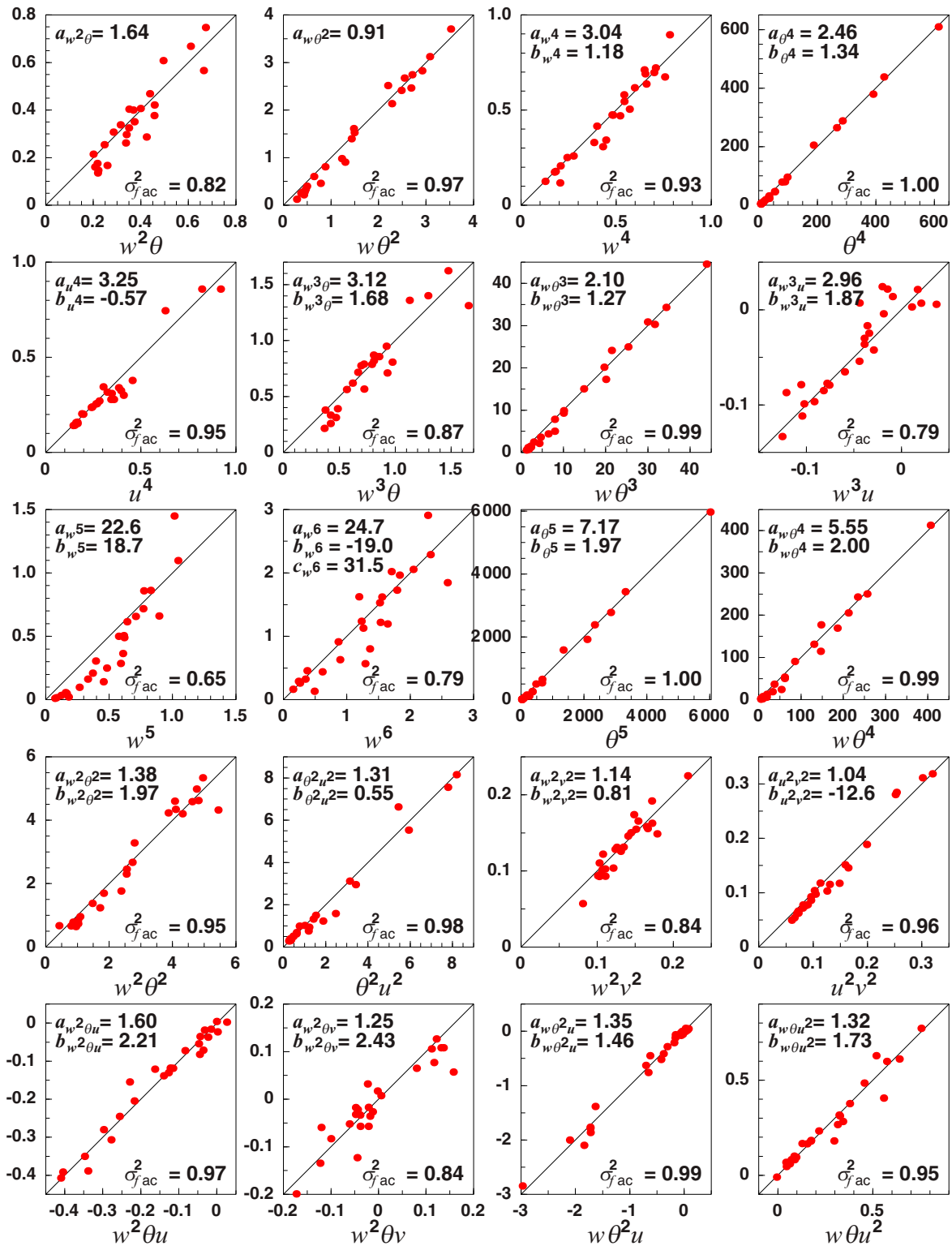
FIG. 10. Selected moments of the semianalytical model ADAM/E with fitted coefficients vs their corresponding measurements from the ARTIST campaign. The abscissas are always the airborne measurements normalized by Deardorff scaling. The ordinates are the ADAM/E moments [Eqs. (53)–(60d)]. In each graph ordinate and abscissa are scaled identically. In the upper-left corner of each panel, the values of the empirical constants are given for the moments fitted to the ARTIST airborne data. In the lower-right corner of each panel the explained variance is given.

the field measurements from the Arctic Radiation and Turbulence Interaction Study (ARTIST) campaign (Hartmann et al. 1999). The available vertical range of the normalized heights for fitting is $z_-/z_i = 0.05$ to $z_+/z_i = 0.95$. Figure 10 shows the high quality of the closure equations.

To specify the values of the empirical constants we use the method of maximization of the explained variance σ^2 (GH02; GH05; Waggy et al. 2016). The explained variance is defined as

$$\sigma^2 = 1 - \frac{\int_{z_-/z_i}^{z_+/z_i} (M_{nmlk} - \langle M_{nmlk} \rangle)^2 \, dz}{\int_{z_-/z_i}^{z_+/z_i} (M_{nmlk} - \hat{M}_{nmlk})^2 \, dz},$$

$$\hat{M}_{nmlk} = \frac{1}{\frac{z_+}{z_i} - \frac{z_-}{z_i}} \int_{z_-/z_i}^{z_+/z_i} M_{nmlk} \, dz, \tag{61}$$

where M_{nmlk} are the measured moments and $\langle M_{nmlk} \rangle$ the ones following from the closure equations. The normalized heights z_-/z_i and z_+/z_i specify the relevant range for optimization. This metrics assesses the ability of the closure equations to correctly describe the results of the measurements and associates the optimal values of the empirical constants with the largest explained variance.

The explained variances range from 0.82 to 1.00 except for $\overline{w'^5}$, where it is only 0.65. Especially high is the explained variance for moments involving the temperature, see the TOM $\overline{w'\theta'^2}$ ($\sigma^2 = 0.97$), FOMs moments $\overline{\theta'^4}$, $\overline{w'\theta'^3}$ ($\sigma^2 = 1.00$, $\sigma^2 = 0.99$), and even fifth-order moments $\overline{\theta'^5}$ ($\sigma^2 = 1.0$) and $\overline{w'\theta'^4}$ ($\sigma^2 = 0.99$).

Interesting to note that trivariate moments, which are TOMs or higher-order moments, are explained even better than some bivariate TOMs and FOMs. The explained variance σ^2 for $\overline{w'^2\theta'}$ is 0.82, for $\overline{w'^3u'}$ is 0.79, while for all of the presented trivariate moments σ^2 is in the range [0.84, 0.99].

Figure 10 also reveals that several constants of ADAM/E are very close to those predicted by ADAM/QN. Thus for coefficients a_{**} we have 0.91 versus 1 for TOM $\overline{w'\theta'^2}$ and 2.96, 3.04, 3.12, and 3.25 versus 3 for the FOMs $\overline{w'^3u'}$,, $\overline{w'^4}$, $\overline{w'^3\theta'}$, and $\overline{u'^4}$, respectively. We stress that this similarity of the Gaussian limit for non-Gaussian closures has nothing in common with the shape of a Gaussian PDF. Most clearly this difference can be seen for the fifth-order moment $\overline{w'\theta'^4}$ ($\sigma^2 = 0.99$). The coefficient $a_{w\theta^4} = 5.55$ versus 6 predicted by ADAM/QN, while the Gaussian moment $\overline{w'\theta'^4} = 0$. Also, several coefficients a_{**} are close to 1 as predicted by ADAM/MF. These are $\overline{u'^2v'^2}$ with $a_{u^2v^2} = 1.04$ and $\overline{w'^2v'^2}$ with $a_{w^2v^2} = 1.14$. This shows that although many of the moments are well described by only a bulk PDF, a shape of the PDF can have a large impact on several moments in the general case. Thus ADAM/E is superior to ADAM/PS, ADAM/QN, and ADAM/MF as expected.

Summarizing, we established a new HOM closure model (ADAM/E) for practical use and derived the empirical constants for this model. Thus, finally, the third and fourth goals of our research are reached.

14. Summary and concluding remarks

Exact solutions of the closure problem are very rare in turbulence theory. We developed an analytically solvable and semianalytical non-Gaussian closure models. All models are derived using the assumed delta-PDF approximation (ADA), focusing on the most robust the bulk properties of any PDF. In this respect the models minimize the number of assumptions, but still capture the most important ingredients of earlier models.

The general quadrivariate assumed delta-PDF approximation model (ADAM) includes four trivariate, six bivariate, and four univariate submodels of lower levels of complexity, see Table 1. All HOMs in this hierarchy have a universal and simple functional form. The analytical closure models have no fitting constants, and the relevant semianalytical HOMs depend on only one, two, or three constants for any HOM. All HOMs are dimensionally consistent and preserve symmetries. The analytical ADAMs are realizable since they have been derived using the same PDF for all moments. For the semianalytical ADAMs, realizability must be checked a posteriori.

The ADAMs show a good skill in predicting the vertical profiles of HOMs for a statistically stationary convective dry atmospheric boundary layer. The profiles of the predicted HOMs have the correct shapes and also the magnitudes are reproduced reasonably well. These are our main results.

The ADAMs are suited for implementation in second-, third-, and fourth-order RANS turbulence closure models of bi-, tri-, and four-variate levels of complexity. If the general ADAMs turn out to be too cumbersome for practical applications in numerical weather prediction and climate models, the trivariate and even bivariate submodels of ADAMs, containing a smaller number of irreducible moments, can be used for such applications. Also, our analysis reveals that several irreducible moments are small in comparison to the other. This opens a door for further simplifications of the ADAMs by reducing the number of relevant moments. The knowledge of the HOMs from the general ADAMs can help to evaluate the accuracy of such simplifications.

As the ADAMs have been developed without moisture consideration, our closure is in the current form only applicable to a dry atmospheric boundary layer, where the effects of moisture can be neglected, or where parameterization schemes distinguish between dry and moist areas. Several moments presented in GH05 and coinciding with those of ADAMs performed well in a wide range of flow regimes in describing the results of deep convection in the ocean (Losch 2004) and in the sun and stars (Kupka and Robinson 2007; Kupka and Muthsam 2017; Cai 2018) and of engineering flows (Waggy et al. 2016; Hsieh and Biringen 2018).

In future studies the capabilities of the ADAMs can be extended by considering different thermodynamic variables, e.g., liquid-water potential temperature θ_l and total suspended water specific humidity q, for moist convective boundary

layers, as well as more scalar variables s, if air pollution mixing is considered. The bottom-up recursive procedure of deriving the closures described in section 3 can be generalized to these cases by enlarging the number of independent variables.

Future work could account for the fluctuations of both structures and background and will require theoretical analysis of subplume (i.e., finite width for delta functions) and interplume (i.e., distribution in positions of delta functions) contributions as well as of an asymmetry of the background (i.e., number of delta functions and its finite width). At the moment these features are only implicitly taken into account in the semianalytical ADAM/S and ADAM/E via the values of empirical constants.

Summarizing, our findings lead us to the conclusion that the new models (ADAMs) exhibit some remarkable and nontrivial properties:

(i) minimization of the number of assumptions in earlier models, but keeping the most important of their properties unchanged,
(ii) the generalization of earlier models to the HOMs,
(iii) the universal functional form of the HOMs,
(iv) the hierarchical structure of the moments of different levels of complexity and
(v) the realizability of all moments for analytical ADAMs, and
(vi) the simplicity of the functional form of all moments, thus being well suited for practical implementations,

which in their qualitative form could survive in more complicated RANS models, and as such form a conceptual basis for understanding convective turbulence in the atmospheric boundary layer, the ocean, in stars and in engineering turbulent flows. The semianalytical version of our closure is based on only one test case. Thus it is obvious that more testing, using different flow regimes, would be desirable. We recommend testing the new closure models, especially ADAM/E, in a priori tests for the full spectrum of HOMs, e.g., in order to establish the best set of empirical constants and to specify the degree of their uncertainty. Also, and more important, a posteriori testing in HOC RANS models is desirable, and even necessary. It is not an easy task because a simple exchange of existing closure implementations might cause difficulties, e.g., due to the need to tune old empirical constants in order to compensate for the effects of the new parameterizations for HOMs.

APPENDIX A

Trivariate HOMs and Closures

Following the guide of solution (section 3), the trivariate HOMs $\langle w'^n \theta'^m u'^l \rangle$ are calculated very similar to the bivariate moments (section 5). The procedure is simple and straightforward: Using Eq. (20) $\langle w'^n \theta'^m u'^l \rangle$ can be written in terms of probabilities and widths as

$$
\begin{aligned}
\langle w'n \theta'^m u'^l \rangle = p_S \Big[& \hat{p}_{uhf}(1 - \hat{p}_u)^n(1 - \hat{p}_h)^m(1 - \hat{p}_f)^l \\
& + \hat{p}_{uhb}(1 - \hat{p}_u)^n(1 - \hat{p}_h)^m(-\hat{p}_f)^l \\
& + \hat{p}_{ucf}(1 - \hat{p}_u)^n(-\hat{p}_h)^m(1 - \hat{p}_f)^l \\
& + \hat{p}_{ucb}(1 - \hat{p}_u)^n(-\hat{p}_h)^m(-\hat{p}_f)^l \\
& + \hat{p}_{dhf}(-\hat{p}_u)^n(1 - \hat{p}_h)^m(1 - \hat{p}_f)^l \\
& + \hat{p}_{dhb}(-\hat{p}_u)^n(1 - \hat{p}_h)^m(-\hat{p}_f)^l \\
& + \hat{p}_{dcf}(-\hat{p}_u)^n(-\hat{p}_h)^m(1 - \hat{p}_f)^l \\
& + \hat{p}_{dcb}(-\hat{p}_u)^n(-\hat{p}_h)^m(-\hat{p}_f)^l \Big] \Delta_w^n \Delta_\theta^m \Delta_u^l. \quad \text{(A1)}
\end{aligned}
$$

Here the expressions for the probabilities $\hat{p}_u$ and $\hat{p}_h$ and for $\hat{p}_f$ are known from the solution for the bivariate moments [Eqs. (26a) and (26b)] and the widths Δ_w, Δ, and Δ_u are given by the formulas (28). To find the probability $\hat{p}_{uhf}$ and similar, we consider the new irreducible moment $\langle w' \theta' u' \rangle$ describing the triple correlations:

$$
\langle w' \theta' u' \rangle = p_S (\hat{p}_{uhf} - \hat{p}_u \hat{p}_{hf} - \hat{p}_h \hat{p}_{uf} - \hat{p}_f \hat{p}_{uh} + 2\hat{p}_u \hat{p}_h \hat{p}_f) \Delta_w \Delta_\theta \Delta_u, \quad \text{(A2)}
$$

where probability $\hat{p}_{uh}$ is defined by (30a) and similar formulas for $\hat{p}_{uf}$ and $\hat{p}_{hf}$, which differ only by a permutation of the indices.

Solving this equation we find the probability $\hat{p}_{uhf}$ as

$$
\hat{p}_{uhf} = \frac{1}{p_S} \frac{\langle w' \theta' u' \rangle}{\Delta_w \Delta_\theta \Delta_u} + \hat{p}_u \frac{\langle \theta' u' \rangle}{\Delta_\theta \Delta_u} + \hat{p}_h \frac{\langle w' u' \rangle}{\Delta_w \Delta_u} + \hat{p}_f \frac{\langle w' \theta' \rangle}{\Delta_w \Delta_\theta} + \hat{p}_u \hat{p}_h \hat{p}_f. \quad \text{(A3a)}
$$

In terms of skewnesses and correlation coefficients this probability reads

$$
\hat{p}_{uhf} = \frac{S_{w-} S_{\theta-} S_{u-} + 4 C_{w\theta} S_{u-} + 4 C_{wu} S_{\theta-} + 4 C_{\theta u} S_{w-} + 8 C_{w\theta u}}{(S_{w+} + S_{w-})(S_{\theta+} + S_{\theta-})(S_{u+} + S_{u-})}. \quad \text{(A3b)}
$$

This equation is obtained by substituting equations for widths (28), probabilities $\hat{p}_u$ (26a), $\hat{p}_h$ (26b), and similarly for $\hat{p}_f$, in Eq. (A3a).

The solutions for the other 7 probabilities is derived by using the relationships for probabilities of different levels of hierarchy, see section 3. They are

$$
\hat{p}_{uhb} = \hat{p}_{uh} - \hat{p}_{uhf}, \quad \text{(A3c)}
$$

$$\hat{p}_{ucf} = \hat{p}_{uf} - \hat{p}_{uhf}, \tag{A3d}$$

$$\hat{p}_{dhf} = \hat{p}_{hf} - \hat{p}_{uhf}, \tag{A3e}$$

$$\hat{p}_{ucb} = \hat{p}_u - \hat{p}_{uh} - \hat{p}_{ucf}, \tag{A3f}$$

$$\hat{p}_{dhb} = \hat{p}_h - \hat{p}_{uh} - \hat{p}_{dhf}, \tag{A3g}$$

$$\hat{p}_{dcf} = \hat{p}_f - \hat{p}_{uf} - \hat{p}_{dhf}, \tag{A3h}$$

$$\hat{p}_{dcb} = 1 - \hat{p}_{uhf} - \hat{p}_{uhb} - \hat{p}_{ucf} - \hat{p}_{ucb} - \hat{p}_{dhf} - \hat{p}_{dhb} - \hat{p}_{dcf}. \tag{A3i}$$

All these probabilities differ from probability (A3b) only by indices, if so they can be derived using the permutation rules for indices similar to the bivariate case.

Finally, substitution of the formulas for all probabilities and widths in Eq. (A1) gives the explicit formula (40) of the main text. This describes any trivariate HOM in terms of three variances, three skewnesses, and three bivariate and one trivariate correlation coefficients.

APPENDIX B

Quadrivariate HOMs and Closures

The quadrivariate HOMs $\langle w'^n \theta'^m u'^l u'^h \rangle$ are calculated very similar to the bivariate and trivariate case, using the factorized form of the HOMs (20). The bottom-up procedure of derivation (see section 3) is applied again, using the results for bivariate closures from section 5 and trivariate closures from appendix A.

The new irreducible moment $\langle w' \theta' u' v' \rangle$, which is necessary for calculation of individual probabilities $\hat{p}_{uhfr}$, is given as

$$\langle w' \theta' u' v' \rangle = p_S (\hat{p}_{uhfr} - \hat{p}_u \hat{p}_{hfr} - \hat{p}_h \hat{p}_{ufr} - \hat{p}_f \hat{p}_{uhr} - \hat{p}_r \hat{p}_{uhf}$$
$$+ \hat{p}_u \hat{p}_h \hat{p}_{fr} + \hat{p}_u \hat{p}_f \hat{p}_{hr} + \hat{p}_u \hat{p}_r \hat{p}_{hf} + \hat{p}_h \hat{p}_f \hat{p}_{ur}$$
$$+ \hat{p}_h \hat{p}_r \hat{p}_{uf} + \hat{p}_f \hat{p}_r \hat{p}_{uh} - 3\hat{p}_u \hat{p}_h \hat{p}_f \hat{p}_r) \Delta_w \Delta_\theta \Delta_u \Delta_v, \tag{B1}$$

where the formulas for all probabilities with the exception of $\hat{p}_{uhfr}$ are given in section 5 and appendix A.

The solution of Eq. (B1) for $\hat{p}_{uhfr}$ gives

$$\hat{p}_{uhfr} = \frac{1}{p_S} \frac{\langle w' \theta' u' v' \rangle}{\Delta_w \Delta_\theta \Delta_u \Delta_v} + \hat{p}_u \frac{\langle \theta' u' v' \rangle}{\Delta_\theta \Delta_u \Delta_v} + \hat{p}_h \frac{\langle w' u' v' \rangle}{\Delta_w \Delta_u \Delta_v} + \hat{p}_f \frac{\langle w' \theta' v' \rangle}{\Delta_w \Delta_\theta \Delta_v}$$
$$+ \hat{p}_r \frac{\langle w' \theta' u' \rangle}{\Delta_w \Delta_\theta \Delta_u} + \hat{p}_u \hat{p}_h \frac{\langle u' v' \rangle}{\Delta_u \Delta_v} + \hat{p}_u \hat{p}_f \frac{\langle \theta' v' \rangle}{\Delta_\theta \Delta_v} + \hat{p}_u \hat{p}_r \frac{\langle \theta' u' \rangle}{\Delta_\theta \Delta_u}$$
$$+ \hat{p}_h \hat{p}_f \frac{\langle w' v' \rangle}{\Delta_w \Delta_v} + \hat{p}_h \hat{p}_r \frac{\langle w' u' \rangle}{\Delta_w \Delta_u} + \hat{p}_f \hat{p}_r \frac{\langle w' \theta' \rangle}{\Delta_w \Delta_\theta} + \hat{p}_u p_h p_f p_r. \tag{B2}$$

The other 15 probabilities are obtained using the generic probability p_{uhfr} and relationships for probabilities of different level of complexity from section 3. The result is as follows:

$$\hat{p}_{uhfl} = \hat{p}_{uhf} - \hat{p}_{uhfr}, \tag{B3a}$$

$$\hat{p}_{uhbr} = \hat{p}_{uhr} - \hat{p}_{uhfr}, \tag{B3b}$$

$$\hat{p}_{ucfr} = \hat{p}_{ufr} - \hat{p}_{uhfr}, \tag{B3c}$$

$$\hat{p}_{dhfr} = \hat{p}_{hfr} - \hat{p}_{uhfr}, \tag{B3d}$$

$$\hat{p}_{uhbl} = \hat{p}_{uh} - \hat{p}_{uhf} - \hat{p}_{uhbr}, \tag{B3e}$$

$$\hat{p}_{ucfl} = \hat{p}_{uf} - \hat{p}_{uhf} - \hat{p}_{ucfr}, \tag{B3f}$$

$$\hat{p}_{ucbr} = \hat{p}_{ur} - \hat{p}_{uhr} - \hat{p}_{ucfr}, \tag{B3g}$$

$$\hat{p}_{dhfl} = \hat{p}_{hf} - \hat{p}_{hfr} - \hat{p}_{uhfl}, \tag{B3h}$$

$$\hat{p}_{dhbr} = \hat{p}_{hr} - \hat{p}_{uhr} - \hat{p}_{dhfr}, \tag{B3i}$$

$$\hat{p}_{dcfr} = \hat{p}_{fr} - \hat{p}_{ufr} - \hat{p}_{dhfr}, \tag{B3j}$$

$$\hat{p}_{ucbl} = \hat{p}_u - \hat{p}_{uh} - \hat{p}_{ucf} - \hat{p}_{ucbr}, \tag{B3k}$$

$$\hat{p}_{dhbl} = \hat{p}_h - \hat{p}_{uh} - \hat{p}_{dhf} - \hat{p}_{dhbr}, \tag{B3l}$$

$$\hat{p}_{dcfl} = \hat{p}_f - \hat{p}_{uf} - \hat{p}_{dhf} - \hat{p}_{dcfr}, \tag{B3m}$$

$$\hat{p}_{dcbr} = \hat{p}_r - \hat{p}_{ur} - \hat{p}_{dhr} - \hat{p}_{dcfr}, \tag{B3n}$$

$$\hat{p}_{dcbl} = 1 - \hat{p}_{uhfr} - \hat{p}_{uhfl} - \hat{p}_{uhbr} - \hat{p}_{uhbl} - \hat{p}_{ucfr} - \hat{p}_{ucbr}$$
$$- \hat{p}_{ucfl} - \hat{p}_{ucbl} - \hat{p}_{dhfr} - \hat{p}_{dhfl} - \hat{p}_{dhbr} - \hat{p}_{dhbl} - \hat{p}_{dcfr}$$
$$- \hat{p}_{dcbr} - \hat{p}_{dcfl}. \tag{B3o}$$

After substituting the formulas for widths and probabilities in the right-hand side of Eq. (20), we find the explicit expression in terms of four skewnesses, six bivariate, four trivariate, and one quadrivariate correlation coefficients. It is the main result, i.e., the Eqs. (44) in the main text.

REFERENCES

Abdella, K., and A. Petersen, 2000: Third-order moment closure through a mass-flux approach. *Bound.-Layer Meteor.*, **95**, 303–318, https://doi.org/10.1023/A:1002629010090.

Cai, T., 2018: Numerical analysis of nonlocal convection–comparison with three-dimensional numerical simulations of efficient turbulent convection. *Astrophys. J.*, **868**, 12, https://doi.org/10.3847/1538-4357/aae1b3.

Canuto, V., F. Minotti, C. Ronchi, R. Ypma, and O. Zeman, 1994: Second-order closure PBL model with new third-order moments: Comparison with LES data. *J. Atmos. Sci.*, **51**, 1605–1618, https://doi.org/10.1175/1520-0469(1994)051<1605:SOCPMW>2.0.CO;2.

Cheng, Y., V. Canuto, and A. Howard, 2005: Nonlocal convective PBL model based on new third- and fourth-order moments. *J. Atmos. Sci.*, **62**, 2189–2204, https://doi.org/10.1175/JAS3474.1.

Cleveland, W. S., 1979: Robust locally weighted regression and smoothing scatterplots. *J. Amer. Stat. Assoc.*, **74**, 829–836, https://doi.org/10.1080/01621459.1979.10481038.

Deardorff, J. W., 1970: Convective velocity and temperature scales for the unstable planetary boundary layer and for Rayleigh convection. *J. Atmos. Sci.*, **27**, 1211–1213, https://doi.org/10.1175/1520-0469(1970)027<1211:CVATSF>2.0.CO;2.

Firl, G. J., and D. A. Randall, 2015: Fitting and analyzing LES using multiple trivariate Gaussians. *J. Atmos. Sci.*, **72**, 1094–1116, https://doi.org/10.1175/JAS-D-14-0192.1.

Gryanik, V. M., and J. Hartmann, 2002: A turbulence closure for the convective boundary layer based on a two-scale mass-flux approach. *J. Atmos. Sci.*, **59**, 2729–2744, https://doi.org/10.1175/1520-0469(2002)059<2729:ATCFTC>2.0.CO;2.

——, ——, S. Raasch, and M. Schröter, 2005: A refinement of the Millionshchikov quasi-normality hypothesis for convective boundary layer turbulence. *J. Atmos. Sci.*, **62**, 2632–2638, https://doi.org/10.1175/JAS3457.1.

Hartmann, J., and Coauthors, 1999: Arctic Radiation and Turbulence Interaction Study (ARTIST). AWI Polar Research Rep. 305, 81 pp.

Hsieh, A., and S. Biringen, 2018: Universality of a higher-order closure model for turbulent rotating flows. *Geophys. Astrophys. Fluid Dyn.*, **112**, 156–164, https://doi.org/10.1080/03091929.2017.1414809.

Hunt, J., 1984: Turbulence structure in thermal convection and shear-free boundary layers. *J. Fluid Mech.*, **138**, 161–184, https://doi.org/10.1017/S0022112084000070.

Ilyushin, B., 2018: Calculation of higher-order moments in the atmospheric boundary layer. *J. Eng. Thermophys.*, **27**, 339–344, https://doi.org/10.1134/S1810232818030098.

Kupka, F., and F. Robinson, 2007: On the effects of coherent structures on higher order moments in models of solar and stellar surface convection. *Mon. Not. Roy. Astron. Soc.*, **374**, 305–322, https://doi.org/10.1111/j.1365-2966.2006.11149.x.

——, and H. J. Muthsam, 2017: Modelling of stellar convection. *Living Rev. Comput. Astrophys.*, **3**, 1, https://doi.org/10.1007/s41115-017-0001-9.

Lappen, C.-L., and D. A. Randall, 2001: Toward a unified parameterization of the boundary layer and moist convection. Part I: A new type of mass-flux model. *J. Atmos. Sci.*, **58**, 2021–2036, https://doi.org/10.1175/1520-0469(2001)058<2021:TAUPOT>2.0.CO;2.

Larson, V. E., and J.-C. Golaz, 2005: Using probability density functions to derive consistent closure relationships among higher-order moments. *Mon. Wea. Rev.*, **133**, 1023–1042, https://doi.org/10.1175/MWR2902.1.

Lenschow, D. H., M. Lothon, S. D. Mayor, P. P. Sullivan, and G. Canut, 2012: A comparison of higher-order vertical velocity moments in the convective boundary layer from lidar with in situ measurements and large-eddy simulation. *Bound.-Layer Meteor.*, **143**, 107–123, https://doi.org/10.1007/s10546-011-9615-3.

Losch, M., 2004: On the validity of the Millionshchikov quasi-normality hypothesis for open-ocean deep convection. *Geophys. Res. Lett.*, **31**, L23301, https://doi.org/10.1029/2004GL021412.

McNicholas, C., and D. Turner, 2014: Characterizing the convective boundary layer turbulence with a high spectral resolution lidar. *J. Geophys. Res. Atmos.*, **119**, 12 910–12 927, https://doi.org/10.1002/2014JD021867.

Mellor, G. L., and T. Yamada, 1982: Development of a turbulence closure model for geophysical fluid problems. *Rev. Geophys.*, **20**, 851–875, https://doi.org/10.1029/RG020i004p00851.

Millionshchikov, M., 1941: On the theory of homogeneous isotropic turbulence. *Dokl. Akad. Nauk SSSR*, **32**, 611–614.

Mironov, D. V., and E. E. Machulskaya, 2017: A turbulence kinetic energy–scalar variance turbulence parameterization scheme. COSMO Tech. Rep. 30, 60 pp.

Monin, A., and A. Yaglom, 2007a: *Statistical Fluid Mechanics: Mechanics of Turbulence.* Vol. I. Dover, 769 pp.

——, and ——, 2007b: *Statistical Fluid Mechanics: Mechanics of Turbulence.* Vol. II. Dover, 874 pp.

Obukhov, A., 1946: Turbulence in an atmosphere with inhomogeneous temperature. *Tr. Inst. Teor. Geofiz. Akad. Nauk SSSR*, **1**, 95–115.

Raasch, S., and M. Schröter, 2001: PALM—A large-eddy simulation model performing on massively parallel computers. *Meteor. Z.*, **10**, 363–372, https://doi.org/10.1127/0941-2948/2001/0010-0363.

Waggy, S. B., A. Hsieh, and S. Biringen, 2016: Modeling higher-order statistics in the turbulent Ekman layer. *Geophys. Astrophys. Fluid Dyn.*, **110**, 391–408, https://doi.org/10.1080/03091929.2016.1196202.

Wyngaard, J., 1987: A physical mechanism for the asymmetry in top-down and bottom-up diffusion. *J. Atmos. Sci.*, **44**, 1083–1087, https://doi.org/10.1175/1520-0469(1987)044<1083:APMFTA>2.0.CO;2.